JCTC Journal of Chemical Theory and Computation

Article

pubs.acs.org/JCTC

Accurate and Efficient Treatment of Continuous Solute Charge Density in the Mean-Field QM/MM Free Energy Calculation

Hiroshi Nakano and Takeshi Yamamoto*

Department of Chemistry, Graduate School of Science, Kyoto University, Kyoto 606-8502, Japan

Supporting Information

ABSTRACT: QM/MM free energy calculation is computationally demanding because of the need for an excessive number of electronic structure calculations. A practical approach for reducing the computational cost is that based on mean field approximation, which calculates the QM wave function in the presence of a partially or totally averaged potential of the MM environment. For obtaining the latter potential, it is common to first represent the QM molecule in terms of point charges and then perform statistical sampling of MM molecules. However, the point charge approximation has the drawback that it tends to overestimate electrostatic (ES) interactions at short-range, which may give rise to a divergence problem in the self-consistent iterations. In this paper, we thus consider a more accurate and robust implementation of mean-field QM/MM method based on continuous QM charge density, here utilizing the following combination: (i) grid-based treatment of ES potential generated by the QM molecule, which allows for an efficient sampling of MM molecules in the presence of QM charge density, and (ii) adaptation of the QM/MM-Ewald method to the mean-field framework for eliminating cutoff errors in the long-range ES interactions. As a numerical test, we apply the obtained method to several benchmark reactions in aqueous solution, and show that the density-based method essentially eliminates the divergence problem while providing the free energy profile consistent with experiment. In addition, we test the utility of a recently proposed screened charge model for the QM charge density and show that the latter also performs well for the free energy calculation. These results suggest that explicit inclusion of charge penetration effects is beneficial for improving the accuracy and stability of the mean-field QM/MM calculation.

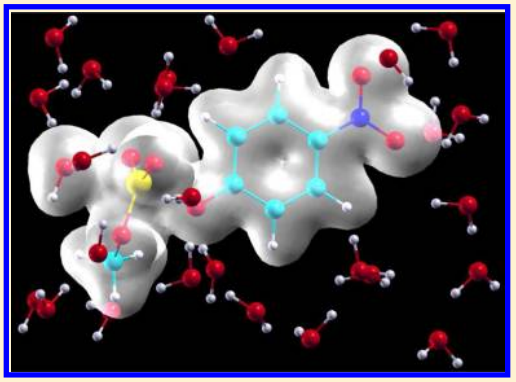

I. INTRODUCTION

The hybrid quantum mechanics/molecular mechanics (QM/MM) methods provide a powerful tool for studying chemical reactions in solution and biological systems.[1−3] They describe the chemically active part of the system quantum mechanically and the rest of the system classically with MM force fields. The computational cost is spent essentially on the QM part, which allows for the use of accurate electronic structure theory for energy calculation. On the other hand, to make a quantitative comparison with experiment, it is often necessary to calculate free energy associated with the reaction of interest. Rigorous or direct calculation of free energy within the QM/MM framework is computationally demanding because the statistical sampling of configuration space involves a large number of QM calculations (say $>10^4$). As such, a variety of approximate methods have been proposed to reduce the computational effort, including the use of ab initio fitted reactive potentials,[3−6] dual-level importance sampling,[4,7−11] interpolated correction,[12,13] and so on.

In this paper, we are particularly interested in a variety of mean-field approximations to the QM wave function. Warshel and co-workers developed an accelerated QM/MM method that evaluated the QM wave function in a partially averaged ensemble of MM configurations.[14,15] In that method, the number of necessary QM calculations is reduced by a factor proportional to the degree of partial MM averaging. The mean field of the MM environment has also been utilized as the zeroth-order part of the QM/MM minimum free energy path method of Yang and co-workers.[16−18] In the limit of an infinite averaging, the accelerated QM/MM method of Warshel and co-workers becomes equivalent to the average solvent electrostatic potential (ASEP) method developed by Aguilar and co-workers.[19−23] In the ASEP method, one calculates the QM wave function in a fully averaged ensemble of MM configurations. Conceptually, this is analogous to the traditional quantum chemical solvation models (such as PCM[24,25] and RISM-SCF methods[26]), which includes the average response field of the environment into the QM Hamiltonian. In a previous paper,[27] we thus explored a theoretical basis for the QM/MM mean-field approximation by starting from the Helmholtz free energy of the total system and then invoking a variational principle of free energy. The resulting formalism was then utilized to calculate the free energy profile of several prototypical reactions in solution.[27,28] It was also demonstrated that the error introduced by the mean-field approximation is

Received: September 25, 2012
Published: November 30, 2012

   dx.doi.org/10.1021/ct300831t | J. Chem. Theory Comput. 2013, 9, 188−203

surprisingly small (less than 1 kcal/mol) when the average distortion of the QM wave function is properly taken into account in the free energy calculation.[27,28] More recently, the mean-field approximation has also been utilized to study enzyme reactions that involve a large conformational change in proteins.[29,30]

All the approximate QM/MM methods mentioned above involve the calculation of a partially[14] or totally[19] averaged MM potential. The average MM potential is usually calculated by first representing the QM molecule in terms of point charges and then performing statistical sampling of the MM environment. The reason for doing so is that it is straightforward to utilize standard MD codes for performing the MM sampling. On the other hand, it is well-known that the point-charge approximation tends to overestimate electrostatic (ES) interactions at short-range, which introduces systematic errors into the calculation. In previous work, Aguilar and co-workers examined the accuracy of point charge approximation by studying a triazene molecule in aqueous solution.[22] They find that the solvent distribution obtained from the mean-field QM/MM calculation (based on point charge approximation) deviates significantly from that obtained from the exact QM/MM calculation. They also demonstrated that adding a few extra point charges on the lone pairs of the QM molecule considerably improves the agreement between the mean-field and exact QM/MM results. A similar discrepancy of solvent distribution was observed for the hydroxide ion in aqueous solution.[31,32] More seriously, in our recent mean-field QM/MM calculation (based on point charge approximation),[28] we encountered a divergence problem during the self-consistent iterations for the phosphoryl dissociation reaction in aqueous solution.[33] This is in contrast to the calculation of the benchmark S_N2 reaction (see Section IV), which proceeds successfully even with the point charge approximation and provides a free energy profile in agreement with the experiment. These observations suggest that the accuracy of point charge approximation depends significantly on the system investigated and care must be taken for its use in the mean-field QM/MM calculation.

As such, the main goal of this paper is to develop a more accurate and robust way to perform mean-field QM/MM calculation based on continuous QM charge density and examine the accuracy and limitation of point charge approximation. To this end, we start by describing the key equations of the mean-field QM/MM method based on QM charge density (Section II.A) and necessary modifications for performing periodic QM/MM calculations (Section II.B). As a numerical test, we apply the obtained method to several benchmark reactions in aqueous solution, namely, prototypical S_N2 reactions, the phosphoryl dissociation reaction, and the hydrolysis of phosphate diester monoanions (Section IV). We discuss the accuracy and limitation of the point charge model by comparison with the density-based result. In addition, we test the utility of a recently proposed screened-charge model for the QM charge density (Section II.C) and demonstrate that in many cases the latter provides as accurate results as the density-based model. The main conclusions thus obtained are summarized in Section V.

II. METHODOLOGY

II.A. Mean-Field QM/MM Free Energy with Continuous Solute Charge Density. We wish to calculate the Helmholtz free energy for a system consisting of one solute molecule and N solvent molecules given by

$$A(\mathbf{R}) = -\frac{1}{\beta}\ln \int d\mathbf{r}^N \exp[-\beta E_{tot}(\mathbf{R}, \mathbf{r})] \tag{1}$$

where $\mathbf{R}$ and $\mathbf{r}^N$ are Cartesian coordinates of the solute and solvent molecules, respectively. The $E_{tot}(\mathbf{R},\mathbf{r})$ is the total energy of the system given by

$$E_{tot}(\mathbf{R}, \mathbf{r}) = \langle\Psi|\hat{H}_0 + \int d\mathbf{x}\hat{\rho}(\mathbf{x})v(\mathbf{x})|\Psi\rangle + E^{vdW}_{QM/MM} + E_{MM} \tag{2}$$

where $\hat{H}_0$ is the Hamiltonian of the solute molecule in the gas phase, $E^{vdW}_{QM/MM}$ is the van der Waals (vdW) interactions between solute and solvent (typically modeled with the Lennard-Jones potential) and E_{MM} is the energy of the solvent molecules. $\hat{\rho}(\mathbf{x})$ is the charge density operator of the QM molecule given by

$$\hat{\rho}(\mathbf{x}) = \sum_a^{nuc} Z_a\delta(\mathbf{x} - \mathbf{R}_a) - \sum_i^{ele} \delta(\mathbf{x} - \mathbf{x}_i) \tag{3}$$

and $v(\mathbf{x})$ is the electrostatic potential (ESP) generated by the MM molecules, namely,

$$v(\mathbf{x}) = \sum_i^{MM} \frac{q_i}{|\mathbf{x} - \mathbf{r}_i|} \tag{4}$$

(In this section we suppose that the system is subject to cluster boundary conditions; see Section II.B for the periodic boundary condition.) In rigorous QM/MM calculation, one solves the following Schrödinger equation

$$[\hat{H}_0 + \int d\mathbf{x}\hat{\rho}(\mathbf{x})v(\mathbf{x})]|\Psi\rangle = E_{eff}|\Psi\rangle \tag{5}$$

for each configuration $(\mathbf{R},\mathbf{r})$. Rigorous calculation of $A(\mathbf{R})$ is expensive because one needs to evaluate $\Psi(\mathbf{R},\mathbf{r})$ for a large number of MM configurations $\mathbf{r}^N$. To avoid this, we consider an approximate QM wave function $\tilde{\Psi}$ that depends only on the solute coordinates $\mathbf{R}$. We suppose that $\tilde{\Psi}(\mathbf{R})$ represents some average or coarse-grained approximation to the original $\Psi(\mathbf{R},\mathbf{r})$. The corresponding total energy may be defined as

$$\tilde{E}_{tot}(\mathbf{R}, \mathbf{r}; \tilde{\Psi}) = \langle\tilde{\Psi}|\hat{H}_0 + \int d\mathbf{x}\hat{\rho}(\mathbf{x})v(\mathbf{x})|\tilde{\Psi}\rangle + E^{vdW}_{QM/MM} + E_{MM} \tag{6}$$

One can then define an approximate QM/MM free energy as

$$\tilde{A}(\mathbf{R}; \tilde{\Psi}) = -\frac{1}{\beta}\ln \int d\mathbf{r}^N \exp[-\beta\tilde{E}_{tot}(\mathbf{R}, \mathbf{r}; \tilde{\Psi})] \tag{7}$$

To determine the optimal $\tilde{\Psi}$, we utilize the inequality

$$E_{tot}(\mathbf{R}, \mathbf{r}) \le \tilde{E}_{tot}(\mathbf{R}, \mathbf{r}; \tilde{\Psi}) \tag{8}$$

which holds true for any $\tilde{\Psi}$ because $\Psi(\mathbf{R}, \mathbf{r})$ is the ground state of the perturbed QM Hamiltonian, $\hat{H}_0 + \int d\mathbf{x}\,\hat{\rho}(\mathbf{x})\,v(\mathbf{x})$, while $\tilde{\Psi}(\mathbf{R})$ is not necessarily so. The above inequality then suggests

$$A(\mathbf{R}) \le \tilde{A}(\mathbf{R}; \tilde{\Psi}) \tag{9}$$

which states that $\tilde{A}(\mathbf{R}; \tilde{\Psi})$ gives an upper bound to the original $A(\mathbf{R})$ irrespective of the choice of $\tilde{\Psi}$. This means that the optimal $\tilde{\Psi}$ is obtained by minimizing $\tilde{A}(\mathbf{R}; \tilde{\Psi})$ with respect to

dx.doi.org/10.1021/ct300831t | J. Chem. Theory Comput. 2013, 9, 188−203

$\tilde{\Psi}$. We write the minimized $\tilde{A}(\mathbf{R}; \tilde{\Psi})$ thus obtained as $A_{\mathrm{MF}}(\mathbf{R})$, that is,

$$A_{\mathrm{MF}}(\mathbf{R}) = \min_{\tilde{\Psi}} \tilde{A}(\mathbf{R}; \tilde{\Psi}) \tag{10}$$

By performing the variational procedure, we obtain the effective Schrödinger equation for $\tilde{\Psi}$ as follows:

$$[\hat{H}_0 + \int \mathrm{d}\mathbf{x}\hat{\rho}(\mathbf{x})\langle v(\mathbf{x})\rangle]|\tilde{\Psi}\rangle = \mathcal{E}_{\mathrm{QM}}|\tilde{\Psi}\rangle \tag{11}$$

where $\langle v(\mathbf{x})\rangle$ is the statistical average of the solvent ESP, with the ensemble average $\langle\cdots\rangle$ defined by

$$\langle\cdots\rangle_{\tilde{\rho}} = \frac{\int \mathrm{d}\mathbf{r}^N \exp[-\beta\mathcal{E}_{\mathrm{MM}}](\cdots)}{\int \mathrm{d}\mathbf{r}^N \exp[-\beta\mathcal{E}_{\mathrm{MM}}]} \tag{12}$$

In eq 12, $\mathcal{E}_{\mathrm{MM}}$ represents the sum of solute−solvent and solvent−solvent interactions in the presence of charge density $\tilde{\rho}$, namely,

$$\mathcal{E}_{\mathrm{MM}}(\mathbf{R}, \mathbf{r}; \tilde{\rho}) = \int \mathrm{d}\mathbf{x}\tilde{\rho}(\mathbf{x})v(\mathbf{x}) + E^{\mathrm{vdW}}_{\mathrm{QM/MM}} + E_{\mathrm{MM}} \tag{13}$$

where $\tilde{\rho}(\mathbf{x})$ is given by

$$\tilde{\rho}(\mathbf{x}) = \langle\tilde{\Psi}|\hat{\rho}(\mathbf{x})|\tilde{\Psi}\rangle \tag{14}$$

Once the $\tilde{\Psi}$ is obtained, we can calculate the mean-field QM/MM free energy as follows:

$$A_{\mathrm{MF}}(\mathbf{R}) = \langle\tilde{\Psi}|\hat{H}_0|\tilde{\Psi}\rangle + \Delta\mu(\mathbf{R}, \tilde{\rho}) \tag{15}$$

where $\Delta\mu$ is the solvation free energy of the solute with fixed $\mathbf{R}$ and $\tilde{\rho}$:

$$\Delta\mu(\mathbf{R}, \tilde{\rho}) = -\frac{1}{\beta}\ln\int \mathrm{d}\mathbf{r}^N \exp[-\beta\mathcal{E}_{\mathrm{MM}}(\mathbf{R}, \mathbf{r}; \tilde{\rho})] \tag{16}$$

Obviously, the above expression for $A_{\mathrm{MF}}(\mathbf{R})$ is analogous to those often employed in the traditional solvation models.[24−26] The essential difference here is that we perform explicit sampling of solvent in order to obtain the average potential. Since the solvation free energy $\Delta\mu$ is calculated explicitly at the molecular level, the above approach may be viewed as intermediate between the rigorous QM/MM calculation and the traditional solvation models.[24−26] We also note that since the effective Schrödinger equation in eq 11 is nonlinear with respect to $\tilde{\Psi}$, one needs to perform the QM calculation of $\tilde{\Psi}$ and the statistical calculation of $\langle v(\mathbf{x})\rangle$ iteratively until self-consistency is reached. This requirement is common to traditional solvation models based on a variational principle of free energy.

II.B. Modification for Periodic QM/MM Systems. In this section, we consider how to modify the above formalism to periodic boundary condition on the basis of the Ewald method. This is important for reactions involving charge separation or migration, because a cutoff-based treatment of ES interactions can introduce nonnegligible errors into the calculated result.[34] In the case of rigorous QM/MM calculation, there exist several well-known approaches for dealing with periodic boundary condition. One such approach is the QM/MM-Ewald method developed by York and co-workers,[34] which was originally utilized with semiempirical QM/MM Hamiltonian. Here, we consider how to combine the basic idea of the QM/MM-Ewald method with the present mean-field framework.

To begin, we separate the simulation box into two spatial regions, called Regions I and II, according to the distance from the QM molecule (see Figure 1). Region I is intended to be the close vicinity of the QM molecule, while Region II represents its complementary part of the simulation box. In this paper, we define Region I as the interior of interlocking spheres centered on each QM atom. The radius of interlocking spheres is chosen sufficiently large so that the ES interaction between the QM molecule and solvent molecules in Region II can be well approximated by point charges. In this paper, the radius of interlocking spheres is chosen as 5 Å, which is sufficiently large for the above criterion. On the other hand, the ES interactions between the QM molecule and solvent molecules in Region I are evaluated more rigorously by inserting MM point charges directly into the Fock matrix of the QM Hamiltonian (see Figure 1).

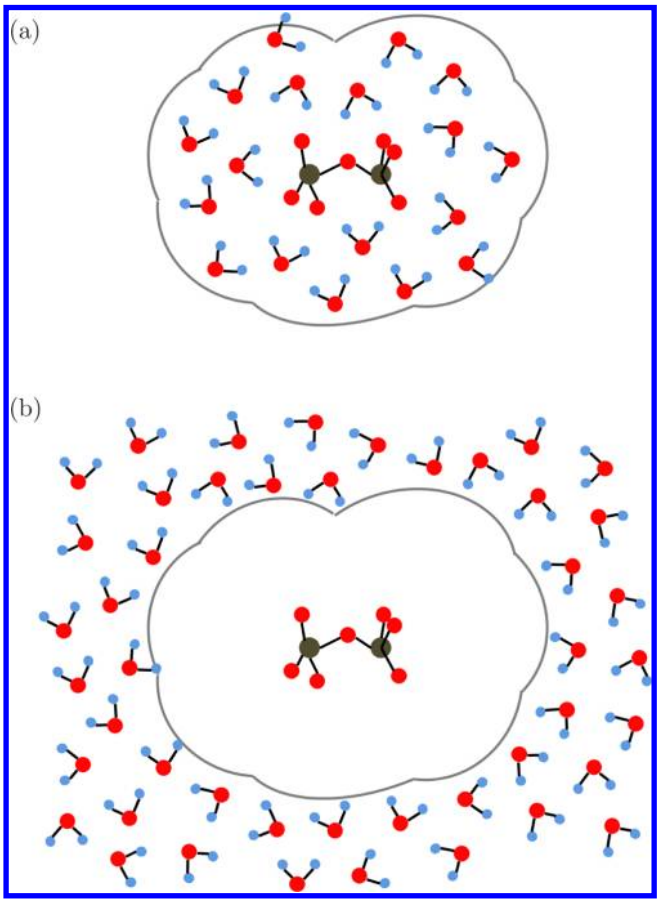

Figure 1. Division of the simulation box into Regions I and II. (a) Region I is defined as the interlocking spheres centered around each QM atom, which include solvent molecules at least in the first solvation shell. (b) Region II represents the complementary part of the simulation box.

Based on the above definition, we consider an approximate total energy of a periodic QM/MM system given by

$$\tilde{E}^{\#}_{\mathrm{tot}}(\mathbf{R}, \mathbf{r}) = \langle\tilde{\Psi}|\hat{H}_0 + \int \mathrm{d}\mathbf{x}\hat{\rho}(\mathbf{x})v^{\mathrm{in}}(\mathbf{x})|\tilde{\Psi}\rangle + \Delta E^{\mathrm{PBC}}(\tilde{\mathbf{Q}}, \mathbf{q}) + E^{\mathrm{vdW}}_{\mathrm{QM/MM}} + E_{\mathrm{MM}} \tag{17}$$

where $\tilde{\Psi}$, $\hat{H}_0$, $\hat{\rho}(\mathbf{x})$, etc., have the same meaning as in Section II.A, and $v^{\mathrm{in}}(\mathbf{x})$ is the ESP generated by solvent molecules in Region I, that is,

$$v^{\mathrm{in}}(\mathbf{x}) = \sum_{i}^{\mathrm{MM(I)}} \frac{q_i}{|\mathbf{x} - \mathbf{r}_i|} \tag{18}$$

The ΔE^{PBC} term in eq 17, which is called the periodic boundary correction (PBC),[34] accounts for all the remaining ES interactions in the periodic system. It may be written as

$$\begin{aligned}\Delta E^{\mathrm{PBC}}(\tilde{\mathbf{Q}}, \mathbf{q}) = &\sum_{a}^{\mathrm{QM}} \sum_{i}^{\mathrm{MM(II)}} \frac{\tilde{Q}_a q_i}{|\mathbf{R}_a - \mathbf{r}_i|} \\ &+ \sum_{a}^{\mathrm{QM}} \sum_{i}^{\mathrm{MM}} \sum_{\mathbf{n}\neq 0} \frac{\tilde{Q}_a q_i}{|\mathbf{R}_a - \mathbf{r}_i + \mathbf{n}L|} \\ &+ \frac{1}{2} \sum_{a}^{\mathrm{QM}} \sum_{b}^{\mathrm{QM}} \sum_{\mathbf{n}\neq 0} \frac{\tilde{Q}_a \tilde{Q}_b}{|\mathbf{R}_a - \mathbf{R}_b + \mathbf{n}L|}\end{aligned} \tag{19}$$

where L is the side length of the simulation box, $\mathbf{n} = (n_x, n_y, n_z)$ is the cell translation vector, and $\tilde{\mathbf{Q}} = \{\tilde{Q}_a\}$ denotes the ESP derived charge of the QM molecule. The first term in the right-hand side represents the ES interactions between the QM molecule and the solvent molecules in Region II. The second term denotes the ES interaction between the QM molecule and the solvent molecules in all the replicated cells (with $\mathbf{n} \neq 0$). The third term is the self-interactions between the QM molecules in the primary and replicated cells. Note that the third term excludes the $\mathbf{n} = 0$ term because it is implicitly accounted for by the QM energy $\langle\tilde{\Psi}|\hat{H}_0|\tilde{\Psi}\rangle$ in eq 17. Now, using the above total energy, we define the mean-field QM/MM free energy under periodic boundary condition as follows:

$$A_{\mathrm{MF}}(\mathbf{R}) = \min_{\tilde{\Psi}} \tilde{A}^{\#}(\mathbf{R}; \tilde{\Psi}) \tag{20}$$

where

$$\tilde{A}^{\#}(\mathbf{R}; \tilde{\Psi}) = -\frac{1}{\beta} \ln \int \mathrm{d}\mathbf{r}^N \exp[-\beta \tilde{E}^{\#}_{\mathrm{tot}}(\mathbf{R}, \mathbf{r}; \tilde{\Psi})] \tag{21}$$

Before proceeding, we note that the minimization of $\tilde{A}^{\#}(\mathbf{R}; \tilde{\Psi})$ in eq 20 should be performed with care, because $\tilde{E}_{\mathrm{tot}}$ in eq 19 depends on QM charge $\tilde{\mathbf{Q}}$ while the latter charge is derived from $\tilde{\Psi}$. To make this dependence explicit, it is useful to write $\tilde{\mathbf{Q}}$ in the form of an expectation value:[35,36]

$$\tilde{Q}_a = \langle\tilde{\Psi}|\hat{Q}_a|\tilde{\Psi}\rangle \tag{22}$$

where $\hat{Q}_a$ is a specific type of population operator that generates ESP charge on QM atom a (see refs 35 and 36, for example, for an explicit expression for $\hat{Q}_a$). Given the latter operator, it is straightforward to perform the minimization of $\tilde{A}^{\#}(\mathbf{R}; \tilde{\Psi})$ with respect to $\tilde{\Psi}$, which gives the effective Schrödinger equation as follows:

$$[\hat{H}_0 + \int \mathrm{d}\mathbf{x}\hat{\rho}(\mathbf{x})\langle v^{\mathrm{in}}(\mathbf{x})\rangle + \sum_a \hat{Q}_a \langle v_a^{\mathrm{out}}\rangle]|\tilde{\Psi}\rangle = \mathcal{E}_{\mathrm{QM}}|\tilde{\Psi}\rangle \tag{23}$$

Here, $v^{\mathrm{in}}(\mathbf{x})$ is the ESP generated by solvent molecules in Region I [see eq 18], while v_a^{out} is the ESP arising from all the molecules outside Region I (in the infinite system), that is,

$$\begin{aligned}v_a^{\mathrm{out}} &= \frac{\partial}{\partial \tilde{Q}_a} \Delta E^{\mathrm{PBC}}(\tilde{\mathbf{Q}}, \mathbf{q}) \\ &= \sum_{i}^{\mathrm{MM(II)}} \frac{q_i}{|\mathbf{R}_a - \mathbf{r}_i|} + \sum_{\mathbf{n}\neq 0} \left\{ \sum_{i}^{\mathrm{MM}} \frac{q_i}{|\mathbf{R}_a - \mathbf{r}_i + \mathbf{n}L|} \right. \\ &\quad \left. + \sum_{b}^{\mathrm{QM}} \frac{\tilde{Q}_b}{|\mathbf{R}_a - \mathbf{R}_b + \mathbf{n}L|} \right\}\end{aligned} \tag{24}$$

Note that the above Schrödinger equation is again nonlinear with respect to $\tilde{\Psi}$, thus requiring an iterative solution. The subsequent argument is essentially the same as in Section II.A, except that the statistical average $\langle\cdots\rangle$ is defined by

$$\langle\cdots\rangle_{\tilde{\rho},\tilde{\mathbf{Q}}} = \frac{\int \mathrm{d}\mathbf{r}^N \exp[-\beta \mathcal{E}^{\#}_{\mathrm{MM}}](\cdots)}{\int \mathrm{d}\mathbf{r}^N \exp[-\beta \mathcal{E}^{\#}_{\mathrm{MM}}]} \tag{25}$$

with the sampling function for the MM part given as

$$\begin{aligned}\mathcal{E}^{\#}_{\mathrm{MM}}(\mathbf{R}, \mathbf{r}) = &\int \mathrm{d}\mathbf{x}\tilde{\rho}(\mathbf{x}) v^{\mathrm{in}}(\mathbf{x}) + \Delta E^{\mathrm{PBC}}(\tilde{\mathbf{Q}}, \mathbf{q}) \\ &+ E^{\mathrm{vdW}}_{\mathrm{QM/MM}} + E_{\mathrm{MM}}\end{aligned} \tag{26}$$

Note that the $\tilde{\rho}(\mathbf{x})$ and $\tilde{\mathbf{Q}}$ are kept fixed during the MD sampling of solvent. The latter sampling is thus "classical" in the sense that the QM calculation is not performed at each time step. More details on practical implementation (including the solution of the effective Schrödinger equation in eq 23) will be discussed in Section III.

II.C. Point-Charge and Screened-Charge Approximations to QM Charge Density. In previous applications of mean-field QM/MM method,[27,28,37] we utilized the point-charge and screened-charge approximations to the QM charge density for the sake of simplicity. In this section, we briefly summarize the key expressions used in those approximations to facilitate comparison with the density-based method. First, in the point-charge (PC) approximation, we describe the solute charge density in terms of ESP charges and assume the following expression for total energy[27,28]

$$\begin{aligned}\tilde{E}^{(\mathrm{pc})}_{\mathrm{tot}}(\mathbf{R}, \mathbf{r}; \tilde{\Psi}) = &\langle\tilde{\Psi}|\hat{H}_0 + \sum_a \hat{Q}_a v_a|\tilde{\Psi}\rangle + E^{\mathrm{vdW}}_{\mathrm{QM/MM}} \\ &+ E_{\mathrm{MM}}\end{aligned} \tag{27}$$

where $\hat{Q}_a$ is the partial charge operator and v_a is the ESP generated by solvent molecules:

$$v_a \equiv v(\mathbf{R}_a) = \sum_{i}^{\mathrm{MM}} \frac{q_i}{|\mathbf{R}_a - \mathbf{r}_i|} \tag{28}$$

(in this section we assume nonperiodic boundary condition for notational simplicity). One can then develop a mean-field QM/MM theory analogous to that described in Section II.A. The effective Schrödinger equation is obtained as[27,28]

$$[\hat{H}_0 + \sum_a \hat{Q}_a \langle v_a\rangle]|\tilde{\Psi}\rangle = \mathcal{E}_{\mathrm{QM}}|\tilde{\Psi}\rangle \tag{29}$$

with the sampling function for the MM part given by

$$\mathcal{E}^{(\mathrm{pc})}_{\mathrm{MM}}(\mathbf{R}, \mathbf{r}) = \sum_a \tilde{Q}_a v_a + E^{\mathrm{vdW}}_{\mathrm{QM/MM}} + E_{\mathrm{MM}} \tag{30}$$

The main advantage of the above PC model is that solute–solvent ES interactions are expressed wholly in terms of point

dx.doi.org/10.1021/ct300831t | J. Chem. Theory Comput. 2013, 9, 188–203

charges, and thus, one can utilize standard MD codes for performing MD calculation. On the other hand, the PC approximation has the well-known drawback that it overestimates the solute−solvent interactions at short-range. To alleviate this problem, we recently developed a type of screened-charge (SC) approximation to QM charge density that is based on the ESP charge operator $\hat{Q}_a$ (ref 37). Specifically, we approximate the charge density operator in eq 3 as follows:

$$\hat{\rho}^{(\mathrm{sc})}(\mathbf{x}) = \sum_a Z_a \delta(\mathbf{x} - \mathbf{R}_a) + \sum_a \hat{Q}_a^{(e)} F_a(\mathbf{x}) \tag{31}$$

where Z_a is the nuclear charge of QM atom a, and $\hat{Q}_a^{(e)}$ is the electronic part of $\hat{Q}$ given by $\hat{Q}_a = Z_a + \hat{Q}_a^{(e)}$. In the above expression, the electronic distribution is approximated by the sum of spherical functions $F_a(\mathbf{x})$ centered on each QM atom. In this paper, we assume a single Slater-type function for $F_a(\mathbf{x})$, that is, $F_a(\mathbf{x}) \sim \exp(-\xi_a|\mathbf{x} - \mathbf{R}_a|)$. Based on the above SC model, one can obtain a slightly different version of mean-field QM/MM theory (see Appendix A), in which the effective Schrödinger equation is

$$[\hat{H}_0 + \sum_a (Z_a\langle v_a\rangle + \hat{Q}_a^{(e)}\langle v_a^F\rangle)]|\tilde{\Psi}\rangle = \mathcal{E}_{\mathrm{QM}}|\tilde{\Psi}\rangle \tag{32}$$

with the sampling function given by

$$\mathcal{E}_{\mathrm{MM}}^{(\mathrm{sc})}(\mathbf{R}, \mathbf{r}) = \sum_a (Z_a v_a + \tilde{Q}_a^{(e)} v_a^F) + E_{\mathrm{QM/MM}}^{\mathrm{vdW}} + E_{\mathrm{MM}} \tag{33}$$

Here, $\tilde{Q}_a^{(e)} = \langle\tilde{\Psi}|\hat{Q}_a^{(e)}|\tilde{\Psi}\rangle$, while v_a^F is the convolution of v_a with the $F_a(\mathbf{x})$ function in eq A5. The main advantage of the above SC model is that it accounts for the charge penetration effects of the QM molecule approximately through the $F_a(\mathbf{x})$ function, while the sampling function in eq 33 retains a simple form of pairwise interactions. This makes the MD calculation as straightforward as in the PC model. We also note that periodic boundary condition can be taken into account by simply calculating v_a and v_a^F with the standard Ewald method.[38] In Section IV we will examine the accuracy of the above PC and SC models by comparing the calculated result with the density-based ones.

III. COMPUTATIONAL DETAILS

III.A. Self-Consistent Calculation of the QM Wave Function and Average MM Potential. In the mean-field QM/MM approach, one needs to calculate the average MM potential by statistically sampling MM molecules. When the QM molecule is represented by its charge density, this is not straightforward because the solute−solvent interactions are not of usual pairwise form (i.e., expressed as the sum of Coulomb and LJ potentials). That is, one needs to calculate the force acting on the solvent molecules numerically at each MD step. What is needed is the electrostatic field $\varphi(\mathbf{x})$ and its gradient $-\nabla\varphi(\mathbf{x})$ arising from the QM charge density, $\tilde{\rho}$. There are two major approaches for this, namely, the solution of the Poisson equation and a direct integration over charge density. In this paper, we choose the latter approach by rewriting the sampling function for the MM part in eq 26 as follows:

$$\mathcal{E}_{\mathrm{MM}}^{\#}(\mathbf{R}, \mathbf{r}) = \sum_i^{\mathrm{MM(I)}} \varphi(\mathbf{r}_i) q_i + \Delta E^{\mathrm{PBC}}(\tilde{\mathbf{Q}}, \mathbf{q}) + E_{\mathrm{QM/MM}}^{\mathrm{vdW}} + E_{\mathrm{MM}} \tag{34}$$

where $\varphi(\mathbf{r}_i)$ denotes the "raw" ESP of the QM molecule defined by

$$\varphi(\mathbf{r}_i) = \int \mathrm{d}\mathbf{x} \frac{\tilde{\rho}(\mathbf{x})}{|\mathbf{r}_i - \mathbf{x}|} \tag{35}$$

Note that the above $\varphi(\mathbf{r}_i)$ is calculated under nonperiodic (or cluster) boundary condition. This is not a problem because the periodicity of the total system is recovered by the PBC term, ΔE^{PBC}. Because of the definition in eq 35, it is straightforward to calculate $\varphi(\mathbf{r}_i)$ using standard quantum chemistry programs given the wave function $\tilde{\Psi}$ or the charge density $\tilde{\rho}$. Another point to note is that in the mean-field QM/MM calculation the $\tilde{\Psi}$ and $\tilde{\rho}$ are invariant during the MD calculation. As a result, the associated ES field $\varphi(\mathbf{x})$ and its gradient $-\nabla\varphi(\mathbf{x})$ are also invariant in the MD calculation. Our strategy is thus to precalculate the values of $\varphi(\mathbf{x})$ over dense grid points in Region I and interpolate them as needed for each solvent molecule. As for the interpolation of $\varphi(\mathbf{x})$, we utilize the third-order Newton-Gregory method:[39]

$$\begin{aligned}\varphi(\mathbf{X}) \simeq{}& \varphi(\mathbf{X}_m) + \sum_i t_i \Delta_i \varphi(\mathbf{X}_m) + \frac{1}{2}\sum_i t_i(t_i - 1) \\ & \Delta_i^2 \varphi(\mathbf{X}_m) + \sum_{i<j} t_i t_j \Delta_i \Delta_j \varphi(\mathbf{X}_m) \\ & + \frac{1}{6}\sum_i t_i(t_i - 1)(t_i - 2)\Delta_i^3 \varphi(\mathbf{X}_m) \\ & + \frac{1}{2}\sum_{i\neq j} t_i t_j (t_j - 1)\Delta_i \Delta_j^2 \varphi(\mathbf{X}_m) + t_x t_y t_z \Delta_x \Delta_y \\ & \Delta_z \varphi(\mathbf{X}_m)\end{aligned} \tag{36}$$

where $\mathbf{X} = \mathbf{X}_m + \sum_{i=x,y,z} t_i h_i \hat{\mathbf{e}}_i$ with t_i, $\hat{\mathbf{e}}_i$, and h_i being the fractional coordinate, the unit vector, and the grid spacing for the ith direction ($i = x,y,z$), respectively. The grid spacing is chosen as 0.2 Å, which is sufficiently small for the present application. The Δ_i in eq 36 is the forward difference operator given by

$$\Delta_i \varphi(\mathbf{X}_m) = \varphi(\mathbf{X}_m + h_i \hat{\mathbf{e}}_i) - \varphi(\mathbf{X}_m) \tag{37}$$

The electric field, $-\nabla\varphi(\mathbf{x})$, was also precalculated on the grid points and interpolated as needed in the MD calculation. In this paper, we span a rectangular grid that closely encompasses Region I, as illustrated by Figure 2 (note that the simulation box is greater than the rectangular grid shown in Figure 2). To save the computational cost, we calculated only the ESP values in Region I using the charge density $\tilde{\rho}$, while those outside Region I with the ESP charges $\tilde{\mathbf{Q}}$. The typical number of grid points inside Region I is 10^4−10^5 (in this paper we did not attempt to minimize the number of grid points). It is interesting to note that unlike spline interpolation, the Newton−Gregory method is a local scheme and thus requires only a small number of grid points around $\mathbf{X}$. As a result, the additional cost for interpolation is rather minor and less than 10% of the total computational time for MD calculation. We also note that the Newton−Gregory method guarantees the

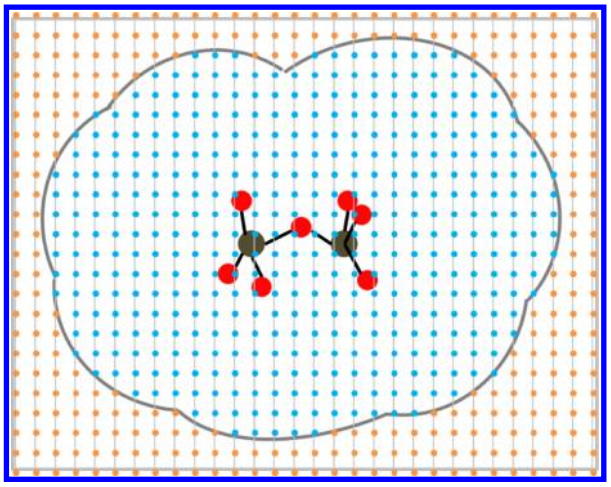

Figure 2. Rectangular grid that encompasses Region I. The ESP of the QM molecule, $\varphi(\mathbf{x})$ in eq 35, is precalculated on the grid points and interpolated on-the-fly during the MD calculation (see text for details). We note that the simulation box (not shown) is larger than the rectangular grid domain shown in the figure.

continuity of an interpolated function over grid points, which leads to good energy conservation in MD calculation.

With the sampling method described above, we calculated the average MM potential as follows:

$$\langle v^{\mathrm{in}}(\mathbf{x})\rangle \simeq \frac{1}{L}\sum_{l=1}^{L}\sum_{i}^{\mathrm{MM(I)}}\frac{q_i}{|\mathbf{x}-\mathbf{r}_i^{(l)}|} \tag{38}$$

$$\langle v_a^{\mathrm{out}}\rangle \simeq \frac{1}{L}\sum_{l=1}^{L} v_a^{\mathrm{out}}(l) \tag{39}$$

where L is the number of MM configurations. Several hundreds of configurations are sufficient to obtain well-converged values of $\langle v^{\mathrm{in}}(\mathbf{x})\rangle$ and $\langle v_a^{\mathrm{out}}\rangle$, provided that those configurations are statistically well decorrelated.[40] In this paper, we generated nearly independent MM configurations by running a single trajectory of 600 ps and selecting $L = 200$ snapshots with equal intervals. We then solve the effective Schrödinger equation in eq 23 by inserting the average MM potential into the QM Hamiltonian. The effect of $\langle v^{\mathrm{in}}(\mathbf{x})\rangle$ was evaluated by inserting each MM point charge in the selected snapshots directly into the Fock matrix of the QM Hamiltonian after multiplying the charge by $1/L$. On the other hand, the effect of $\langle v_a^{\mathrm{out}}\rangle$ was included into the QM Hamiltonian by use of the ESP charge operator, $\hat{Q}_a$. For this purpose, we utilized a locally modified version of the GAMESS program[41] in which the ESP charge operator has been implemented. For each solute geometry $\mathbf{R}$, we repeated the QM calculation of $\tilde{\Psi}$ and the MD sampling of solvent typically 4−5 times until self-consistency was achieved. That is, we optimized the mean-field wave function self-consistently at each value of the reaction coordinate. The other protocol of the MD simulation is as follows: The system consisted of one solute molecule and 860 water molecules described by the TIP3P model.[42] The LJ parameters were taken from the AMBER94[43] and OPLS-AA[44] force fields, except that the parameter for the chloride ion was taken from Gao and Xia.[45] All the MD calculations were performed with a locally modified version of the DL_POLY MD program in which the Newton−Gregory interpolation in eq 35 has been implemented. The temperature was kept at 298 K, and the size of the simulation box was determined from a separate NPT run at 1 atm. As described in Section II.B, all the ES interactions were evaluated with the Ewald method. The explicit Ewald expression for the ΔE^{PBC} term in eq 19 is given in Appendix C.

III.B. Potential of Mean Force Profile. In the following sections, we apply the above method to several benchmark reactions in solution. Specifically, we calculate the potential of mean force (PMF) profile by integrating the free energy gradient, $\nabla A_{\mathrm{MF}}(\mathbf{R})$, along a given reaction path. The free energy gradient is evaluated by using the following expression (see Appendix B for the derivation):

$$\frac{\partial}{\partial \mathbf{R}}A_{\mathrm{MF}}(\mathbf{R}) = \left.\frac{\partial \mathcal{E}_{\mathrm{QM}}(\mathbf{R}, \bar{v}^{\mathrm{in}}, \bar{v}^{\mathrm{out}})}{\partial \mathbf{R}}\right|_{\bar{v}^{\mathrm{in}},\bar{v}^{\mathrm{out}}} + \left\langle \frac{\partial}{\partial \mathbf{R}}(\Delta E^{\mathrm{PBC}} + E_{\mathrm{QM/MM}}^{\mathrm{vdW}})\right\rangle_{\tilde{\rho},\tilde{\mathbf{Q}}} \tag{40}$$

where $\bar{v}^{\mathrm{in}} = \langle v^{\mathrm{in}}(\mathbf{x})\rangle$ and $\bar{v}^{\mathrm{out}} = \langle v^{\mathrm{out}}\rangle$. Note that the first term in eq 40 is evaluated at fixed $\bar{v}^{\mathrm{in}}$ and $\bar{v}^{\mathrm{out}}$, while the second term at fixed $\tilde{\rho}$ and $\tilde{\mathbf{Q}}$. The integration of the free energy gradient is performed as follows,

$$A_{\mathrm{MF}}(\mathbf{R}_*(\xi)) = \int_{\xi_0}^{\xi} \mathrm{d}\xi' \left.\frac{\partial A_{\mathrm{MF}}(\mathbf{R})}{\partial \mathbf{R}}\right|_{\mathbf{R}=\mathbf{R}_*(\xi')} \cdot \frac{\mathrm{d}\mathbf{R}_*(\xi')}{\mathrm{d}\xi'} + \mathrm{const} \tag{41}$$

where $\mathbf{R}_*(\xi)$ denotes the solute coordinates on the reaction path. In practice, we evaluate the above integral approximately as

$$A_{\mathrm{MF}}(\mathbf{R}_*(\xi_K)) - A_{\mathrm{MF}}(\mathbf{R}_*(\xi_0)) \simeq \sum_{k=1,K}\frac{1}{2}[\nabla A_{\mathrm{MF}}(\mathbf{R}_*(\xi_k)) + \nabla A_{\mathrm{MF}}(\mathbf{R}_*(\xi_{k-1}))] [\mathbf{R}_*(\xi_k) - \mathbf{R}_*(\xi_{k-1})] \tag{42}$$

where $\{\xi_k\}$ are equally spaced grid points of the reaction coordinate. The grid spacing of ξ_k is chosen as 0.2 Å, which is sufficiently small for the present applications. For the S_N2 reactions studied in Section IV, we utilize the reaction path obtained from our previous mean-field QM/MM calculation.[28] On each of the path, the QM geometry was optimized with the reaction coordinate fixed at a specific value ξ_k. In the latter study, the reaction coordinate is chosen as

$$\xi = r(\mathrm{Cl} - \mathrm{C}) - r(\mathrm{C} - \mathrm{Cl}') \tag{43}$$

for the Finkelstein reaction and

$$\xi = r(\mathrm{Cl} - \mathrm{C}) - r(\mathrm{C} - \mathrm{N}) \tag{44}$$

for the Menshutkin reaction; see Section IV for more details on the reaction path.

IV. APPLICATION TO BENCHMARK REACTIONS IN SOLUTION

IV.A. Type-I S_N2 (Finkelstein) Reaction. We first apply the above method to the Type-I S_N2 (Finkelstein) reaction

$$\mathrm{Cl}^- + \mathrm{CH_3Cl} \rightarrow \mathrm{ClCH_3} + \mathrm{Cl}^- \tag{45}$$

which exhibits charge displacement from the attacking chloride ion to the leaving one as the reaction proceeds. Since the reactants have a more localized charge distribution than the transition state, a polar solvent stabilizes the former more

dx.doi.org/10.1021/ct300831t | J. Chem. Theory Comput. 2013, 9, 188−203

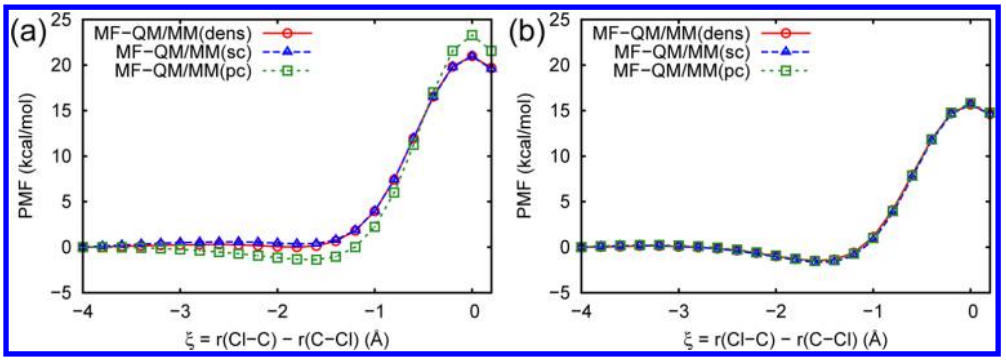

Figure 3. Potential of mean force (PMF) profile of the Finkelstein reaction $Cl^- + CH_3Cl \rightarrow ClCH_3 + Cl^-$ (a) in water and (b) in acetonitrile solution. The PMF profiles are calculated with the mean-field QM/MM method based on continuous solute charge density [denoted as MF-QM/MM(dens)], its screened-charge approximation [MF-QM/MM(sc)], and point-charge approximation [MF-QM/MM(pc)]. The QM calculation is performed at the BHHLYP/6-31+G(d,p) level.

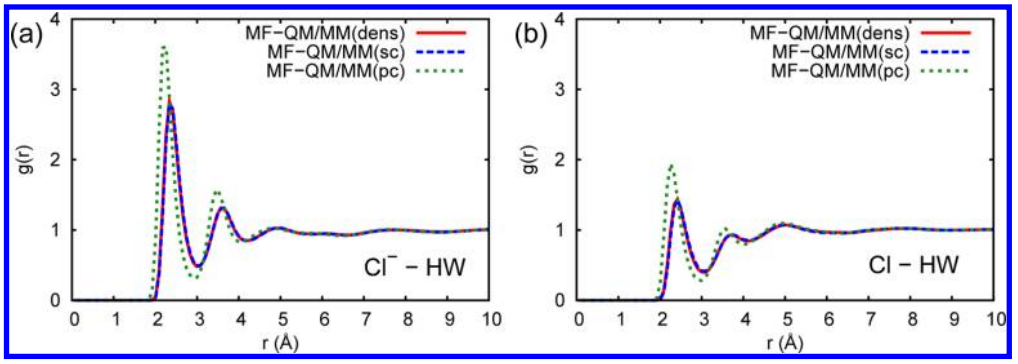

Figure 4. Radial distribution functions (RDFs) of water hydrogen around the solute molecule of the Finkelstein reaction in water obtained from the mean-field QM/MM calculation: (a) $\xi = -4.0$ Å (reactant), (b) $\xi = 0.0$ Å (transition state).

strongly than the latter, making the free energy barrier higher in polar solvents. Indeed, it is known that the Finkelstein reaction proceeds by orders of magnitude slower in polar solvents than in the gas phase.[46] Because of this, the Finkelstein reaction has been studied extensively using a variety of theoretical methods.[17,28,47−59]

Figure 3a displays the profile of $A_{MF}(\mathbf{R})$ obtained from mean-field QM/MM calculation with continuous charge density (labeled as MF-QM/MM(dens)), the PC model (MF-QM/MM(pc)), and the SC model (MF-QM/MM(sc)). The level of QM calculation is chosen as BHHLYP/6-31+G(d,p), which gives an accurate energy profile in the gas phase close to the CCSD(T) result (see Figure 1 in ref 28). The barrier height of $A_{MF}(\mathbf{R})$ obtained from the density-based calculation is $\Delta A^{\ddagger} = 21.0$ kcal/mol, which is rather similar to that obtained with the PC model, $\Delta A^{\ddagger} = 23.3$ kcal/mol. The SC model gives the PMF profile essentially identical to the density-based result. To compare the calculated value with experiment, it is necessary to add solute thermal/entropic correction because the solute geometry is fixed in the PMF calculation. In a previous work,[28] we estimated the latter using the standard separable rotation/vibration approximation, which gives $\Delta A_{slt} = 4.0$ kcal/mol. By adding the latter value, we can estimate the activation free energy as 21.0 + 4.0 = 25.0 kcal/mol, which agrees well with the experimental result[60] (26.6 kcal/mol). The agreement may be somewhat improved by using the CCSD(T) method for the QM molecule, because the gas-phase barrier at the CCSD(T) level is 1−2 kcal/mol higher than that at the BHHLYP level.[28] Before proceeding, we note that the PMF profiles shown in Figure 3 are statistically well converged, with the standard deviation of the barrier height being about 0.3 kcal/mol (see the Supporting Information).

Figure 4 displays the radial distribution functions (RDFs) obtained from the MF-QM/MM calculation. As seen, the PC model overestimates the solvation of the chloride atom of the solute molecule as compared to the density-based result. This is not surprising because the present PC model is known to overestimate the solute−solvent interactions at short-range, particularly for solvated anions.[37] This is in contrast to the SC model, which yields the RDF in excellent agreement with the density-based result. Figure 5 displays the corresponding spatial distribution functions (SDFs) of water molecules. As expected, the SDFs obtained with the density-based and SC models are similar to each other, while the PC model overestimates the solvent distribution around the chloride ion.

To be more quantitative about the error introduced by the PC model, we calculated the solvation free energy of the solute molecule. Since the three charge models differ only in the treatment of electrostatic interactions, we examined only the ES contribution to solvation free energy given by

$$\Delta\mu_{es} = -\frac{1}{\beta}\ln\frac{\int d\mathbf{r}^N \exp\{-\beta\mathcal{E}_{MM}\}}{\int d\mathbf{r}^N \exp\{-\beta\mathcal{E}^0_{MM}\}} \tag{46}$$

Here, $\mathcal{E}_{MM}(\mathbf{R}, \mathbf{r})$ is the sampling function for MM part [e.g., eq 26], and $\mathcal{E}^0_{MM}(\mathbf{R}, \mathbf{r})$ is the nonelectrostatic contribution given by $\mathcal{E}^0_{MM} = E^{vdW}_{QM/MM} + E_{MM}$. We evaluated the above $\Delta\mu_{es}$ by using linear response approximation:[61]

$$\Delta\mu^{(dens)}_{es} \simeq \frac{1}{2}\int d\mathbf{x}\tilde{\rho}(\mathbf{x})\langle v(\mathbf{x})\rangle \tag{47a}$$

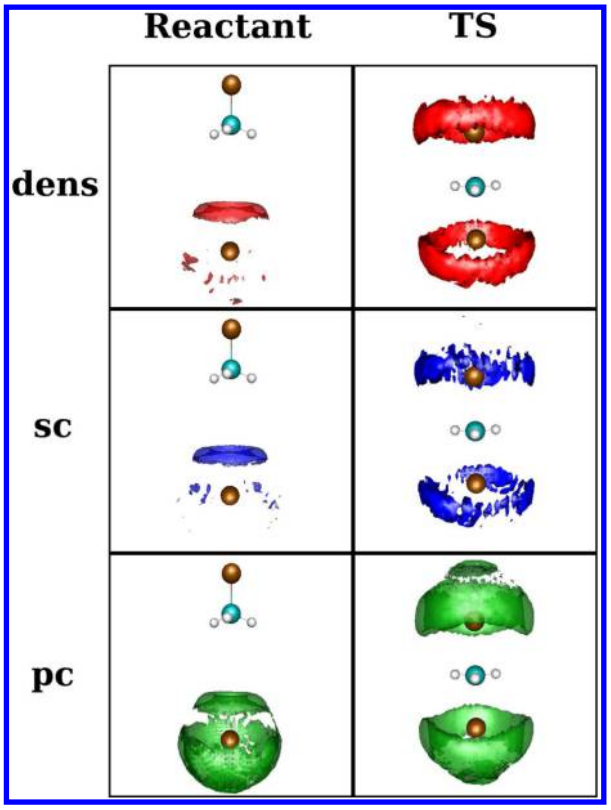

Figure 5. Spatial distribution functions (SDFs) of water hydrogen around the solute molecule of the Finkelstein reaction in water obtained from the mean-field QM/MM calculation: (left column) reactant state with $\xi = -4.0$ Å, (right column) transition state with $\xi = 0.0$ Å. For the reactant state (transition state), the isosurfaces are plotted for the number density of 0.20 (0.15) Å^{-3}, which is equivalent to 3.1 (2.3) times the average number density of water hydrogen.

$$\Delta\mu_{es}^{(sc)} \simeq \frac{1}{2}\sum_a [Z_a\langle v_a\rangle + \tilde{Q}_a^{(e)}\langle v_a^F\rangle] \tag{47b}$$

$$\Delta\mu_{es}^{(pc)} \simeq \frac{1}{2}\sum_a \tilde{Q}_a\langle v_a\rangle \tag{47c}$$

The calculated values of $\Delta\mu_{es}$ are summarized in Table 1. For the reactant state ($\xi = -4.0$ Å), the value of $\Delta\mu_{es}$ obtained with the PC model (−95.6 kcal/mol) differs considerably from that obtained with the SC model (−82.2 kcal/mol) or the density-based model (−84.4 kcal/mol). A similar discrepancy is observed for the transition state ($\xi = 0.0$ Å). Namely, the $\Delta\mu_{es}$ obtained with the PC model (−80.6 kcal/mol) is rather different from the SC (−68.0 kcal/mol) and density-based (−68.2 kcal/mol) results. On the other hand, it is interesting to note that the difference of $\Delta\mu_{es}$ between the reactant and transition state [namely, $\Delta\Delta\mu_{es} = \Delta\mu_{es}(\xi = 0.0) - \Delta\mu_{es}(\xi = -4.0)$ = 15.0, 14.2, and 16.2 kcal/mol for the PC, SC, and density-based models, respectively] are rather insensitive to the choice of different charge models. This fact implies that the errors introduced by the different charge models tend to cancel along the reaction coordinate, which leads to the rather similar PMF profiles shown in Figure 3. This point will be discussed further in Section IV.B.

Table 1. Electrostatic Component of Solvation Free Energy $\Delta\mu_{es}$ (in kcal/mol) for the Finkelstein Reaction $Cl^- + CH_3Cl \rightarrow ClCH_3 + Cl^-$ in Water and Acetonitrile Solution[a]

	PC	SC	dens
	Water		
RS	−95.6	−82.2	−84.4
TS	−80.6	−68.0	−68.2
$\Delta\Delta\mu_{es}$	15.0	14.2	16.2
	Acetonitrile		
RS	−59.0	−57.6	−57.8
TS	−48.7	−47.6	−47.7
$\Delta\Delta\mu_{es}$	10.3	10.0	10.1

[a] $\Delta\mu_{es}$ is calculated for the reactant state (RS) with $\xi = -4.0$ Å and the transition state (TS) with $\xi = 0.0$ Å. Their difference is denoted as $\Delta\Delta\mu_{es} \equiv \Delta\mu_{es}(TS) - \Delta\mu_{es}(RS)$. "PC", "SC", and "dens" stand for the MF-QM/MM calculation based on the point-charge, screened-charge, and density-based models, respectively.

The situation becomes quite different for reactions in nonaqueous solution. This is illustrated by the PMF profile for the Finkelstein reaction in acetonitrile solution. The latter is obtained with the same computational protocol except that the Böhm model[62] is used for the solvent. Figure 3b displays the obtained PMF, which exhibits a lower barrier ($\Delta A^{\ddagger}$ = 15.7 kcal/mol) than in aqueous solution by reflecting the smaller polarity of acetonitrile. More importantly, Figure 3b shows that all the charge models provide essentially the identical PMF profiles. This fact suggests that charge penetration effects of the solute molecule are not particularly important for acetonitrile solution. Table 1 shows the same trend (i.e., the three charge models provide similar values of $\Delta\mu_{es}$). Therefore, the limited accuracy of the PC model is of more concern for aqueous solution (where solute−solvent hydrogen bonds may exist) than for nonaqueous solution such as acetonitrile.

IV.B. Type-II S_N2 (Menshutkin) Reaction. We next consider the Type-II S_N2 (Menshutkin) reaction,

$$NH_3 + CH_3Cl \rightarrow NH_3CH_3^+ + Cl^- \tag{48}$$

which is unusual in that the reactants are neutral molecules while the products are an ion pair. The PMF profile thus depends significantly on the type of the environment. For example, the PMF is strongly endergonic in the gas phase due to Coulomb attraction between the product ions, while it becomes strongly exergonic in aqueous solution because of the solvation of products by water molecules. As such, the Menshutkin reaction has often been employed as a good system for testing new theoretical methods.[13,21,27,28,45,63−72]

Figure 6a displays the PMF profile obtained from the MF-QM/MM calculation. The QM level is chosen as MP2/6-31+G(d,p), which gives an accurate energy profile similar to the CCSD(T) result (see Supporting Information). The PMF profiles obtained with the density-based and SC models are very similar. The barrier height $\Delta A^{\ddagger}$ and reaction free energy ΔA_r obtained with the density-based model are 16.7 and −25.8 kcal/mol, respectively. On the other hand, the PC model predicts a more exergonic PMF profile with ΔA_r=−31.7 kcal/mol. The reason is essentially attributed to the overestimated solvation of the product ions (see the Supporting Information for relevant RDFs). For comparison, we also calculated the PMF in acetonitrile solution using the same computational protocol (Figure 6b). The PMF in acetonitrile solution is less exergonic than in aqueous solution due to weaker solvation of the product ions. More importantly, we see that all the charge models provide essentially the same PMF profile, which

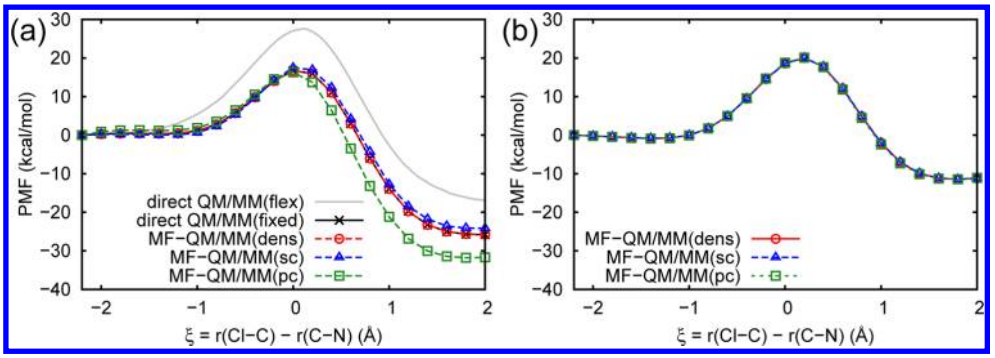

Figure 6. PMF profile of the Menshutkin reaction $NH_3 + CH_3Cl \rightarrow NH_3CH_3^+ + Cl^-$ (a) in water and (b) in acetonitrile solution obtained from the mean-field QM/MM calculation. The PMF obtained from the direct QM/MM calculations are also shown for comparison (see the main text for details). The QM calculation is performed at the MP2/6-31+G(d,p) level.

indicates that the PC model is sufficiently accurate for the Menshutkin reaction in nonaqueous solution.

As is clear from Section II, the mean-field QM/MM method totally neglects statistical fluctuations of the QM wave function about the self-consistent state. To examine the impact of this mean-field approximation, we performed two types of rigorous QM/MM calculations for comparison. In the first type of calculation, we calculated the QM/MM free energy gradient as follows,

$$\frac{\partial A(\mathbf{R})}{\partial \mathbf{R}} = \left\langle \frac{\partial E_{\mathrm{tot}}(\mathbf{R}, \mathbf{r})}{\partial \mathbf{R}} \right\rangle \tag{49}$$

where E_{tot} is the total energy given by eq 2. The ensemble average was calculated by running a QM/MM trajectory of 120 ps, with the QM wave function evaluated at each MD time step. It should be noted that, in the trajectory calculation, the solute molecule was fixed at a given geometry on the reaction path, $\mathbf{R}(\xi)$. The above calculation was repeated for 22 grid points of ξ_k, involving a total of 2640-ps QM/MM trajectory run. By integrating the free energy gradient thus evaluated, we obtain the PMF profile shown in Figure 6a [labeled as "direct QM/MM(fixed)"]. Remarkably, the direct PMF thus obtained agrees quantitatively with that obtained from the MF-QM/MM(dens) calculation. This fact indicates that the neglect of fluctuations in the QM wave function (about the self-consistent state) does not introduce significant errors into the PMF. The latter conclusion is consistent with a similar comparison for the Finkelstein reaction in aqueous solution.[28]

The above direct QM/MM calculation is not conventional in that the solute molecule is fixed in space during the trajectory calculation. A more standard approach is to move all the degrees of freedom other than the reaction coordinate $\xi(\mathbf{R})$. The corresponding PMF is given by

$$G(\xi') = -\frac{1}{\beta} \ln \int \mathrm{d}\mathbf{R} \int \mathrm{d}\mathbf{r}^N \exp[-\beta E_{\mathrm{tot}}(\mathbf{R}, \mathbf{r})] \times \delta[\xi(\mathbf{R}) - \xi'] \tag{50}$$

For comparison, we also calculated the above $G(\xi')$ by performing a series of umbrella sampling followed by the weighted histogram analysis. Here, the umbrella potential was defined for each grid point of $\{\xi_k\}$ $(1 \le k \le 22)$ with an equal spacing of 0.2 Å and appropriate force constant.[73] For each umbrella potential, we performed a direct QM/MM sampling for 80 ps, thus running a total of 1760 ps QM/MM calculation to obtain a single PMF. The result is shown in Figure 6a [labeled as "direct QM/MM(flex)"]. The free energy of activation and reaction thus obtained is $\Delta G^{\ddagger} = 27.6$ and $\Delta G_r = -16.9$ kcal/mol, respectively. To compare these values with the MF-QM/MM result, it is necessary to add solute thermal correction, ΔA_{slt}. We estimated the latter using the separable rotation/vibration approximation[74−76] at the MP2/6-31+G(d,p)/COSMO level. The free energy of activation and reaction thus obtained from the MF-QM/MM(dens) calculation (with solute thermal correction) is $\Delta G^{\ddagger} = 16.7 + 9.2 = 25.9$ and $\Delta G_r = -25.8 + 7.7 = -18.1$ kcal/mol, respectively, which agree reasonably well with the direct QM/MM results obtained above (27.6 and −16.9 kcal/mol). The above estimate of $\Delta G^{\ddagger}$ is also in good agreement with $\Delta G^{\ddagger} = 25.6$ kcal/mol obtained previously with the ASEP/MD method at the BHHLYP level.[21] We now want to compare the calculated values of $\Delta G^{\ddagger}$ and ΔG_r with experiment. However, experimental data for $\Delta G^{\ddagger}$ do not appear to be available for the reaction in eq 48. For comparison, $\Delta G^{\ddagger}$ for an analogous reaction $NH_3 + CH_3I \rightarrow NH_3CH_3^+ + I^-$ in water is known to be 23.5 kcal/mol.[45] On the other hand, the experimental value of ΔG_r for the reaction eq 48 is $\Delta G_r = -34 \pm 10$ kcal/mol.[45] Thus, the present estimate of ΔG_r obtained from the MF-QM/MM(dens) calculation is close to the upper limit of the uncertainty of the experimental result. It is not clear at present whether the above deviation between theory and experiment is attributed to the insufficient accuracy of the present QM/MM model or the rather large error bar of the experimental result.

C. Phosphoryl Dissociation Reaction. We now consider the dissociation reaction of methyl phosphate dianion in aqueous solution

$$CH_3OPO_3^{2-} \rightarrow CH_3O^- + PO_3^- \tag{51}$$

as an example of highly charged systems. This reaction has been studied experimentally as a model of phosphoryl transfer ubiquitous in biological systems.[77−79] York and co-workers[34] studied the above reaction by using the QM/MM-Ewald method at the semiempirical level and demonstrated that a cutoff-based treatment introduces significant errors into the obtained PMF. In a previous work,[28] we also studied the above reaction by using the MF-QM/MM(pc) method but encountered a divergence problem during the self-consistent iterations. This problem is qualitatively similar to the so-called polarization catastrophe in polarizable simulations, and thus, it may be avoided by explicitly accounting for charge penetration effects.

To see whether this is the case, we performed the MF-QM/MM calculation based on continuous charge density (Figure 7). The reaction path was taken from our previous work.[28] The

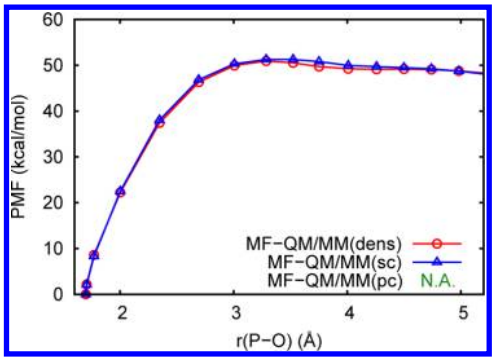

Figure 7. PMF profile of the phosphoryl dissociation reaction $CH_3OPO_3^{2-} \rightarrow CH_3O^- + PO_3^-$ in aqueous solution obtained from the mean-field QM/MM calculation. The PMF for the MF-QM/MM(pc) calculation is not available because of the divergent behavior of ESP derived charges in the PC model. The QM calculation is performed at the MP2/6-31+G(d,p) level.

QM level is chosen as the MP2/6-31+G(d,p) level, which is sufficiently accurate compared to the CCSD(T) result (see the Supporting Information). As expected, the density-based calculation exhibited no divergence problem, providing a well-defined PMF. The SC model also converged successfully and provided the PMF similar to the density-based result (Figure 7). On the other hand, the PC model exhibited a divergence problem and failed to obtain the corresponding PMF. These results confirm that explicit inclusion of charge penetration effects is crucial for describing the reaction in eq 51. The barrier height thus obtained from the density-based calculation is $\Delta A^{\ddagger} = 50.9$ kcal/mol, and the reaction free energy (as estimated from the right edge of the PMF profile) is $\Delta A_r = 48.3$ kcal/mol. We can compare these values with experiment by adding solute thermal correction, ΔA_{slt}, which was again estimated using the separable rotation/vibration approximation at the BHHLYP/6-31+G(d,p)/COSMO level.[80] The resulting estimate of activation free energy is $\Delta G^{\ddagger} = 50.9 - 5.4 = 45.5$ kcal/mol, and the reaction free energy is $\Delta G_r = 48.3 - 13.0 = 35.3$ kcal/mol. The experimental reaction free energy is known to be 37 ± 3 kcal/mol (ref 79), which agrees well with the calculated result (35.3 kcal/mol). The experimental activation free energy for the hydrolysis of methyl monophosphate dianion (MMP^{2-}) is known to be $\Delta G^{\ddagger} = 44$ kcal/mol (ref 81), which compares favorably with the present MF-QM/MM result (45.5 kcal/mol). However, the latter comparison should be regarded as qualitative, because the mechanism of the hydrolysis reaction of MMP^{2-} has not been elucidated experimentally. A previous theoretical study using the COSMO solvation model[82] indicates that the hydrolysis of MMP^{2-} proceeds via the associative mechanism rather than the dissociative one. On the other hand, a recent study at the QM/MM level suggests that the free energy surface is rather flat around the transition state and consequently the two mechanisms are virtually indistinguishable.[83] If the latter is the case, the relatively good agreement of $\Delta G^{\ddagger}$ between the present and experimental results may be reasonable.

Figure 8 displays the SDF of water molecules around the solute molecule. The corresponding RDFs are shown in the Supporting Information. In the reactant state, the solute has a net charge of $-2e$ and is strongly solvated by water molecules. As the reaction proceeds, the solute molecule separates into the methoxide (CH_3O^-) and metaphosphate (PO_3^-) ions. Since the net charge of the reactant is greater than that of product ions, the solvation of the former is stronger than the latter, which is reflected in the greater excess population of solvent in the reactant state. In the product state, the excess distribution of water is much more evident around the methoxide ion than the metaphosphate ion. This is because the net charge of the methoxide ion is essentially localized on the terminal oxygen atom, while the charge of the metaphosphate ion is delocalized over three oxygen atoms. Regarding the comparison between different charge models, we see that the SC model slightly underestimates the solvation as compared to the density-based model, although their difference is rather small.

IV.D. Hydroxide Attack on Phosphate Diester Monoanion. Finally, we consider the hydrolysis of phosphate diester monoanions by the attack of a hydroxide ion in water,

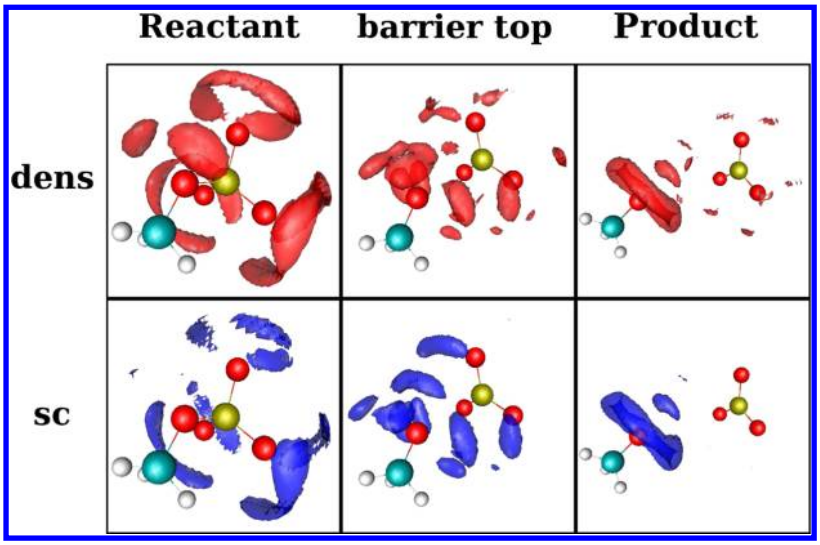

Figure 8. SDFs of water hydrogen around the solute molecule of the phosphoryl dissociation reaction in aqueous solution. The isosurfaces are plotted for the number density of 0.50 $Å^{-3}$, which is equivalent to 7.7 times the average number density of water hydrogen. "dens" and "sc" indicate the results obtained from the MF-QM/MM(dens) and MF-QM/MM(sc) calculations, respectively.

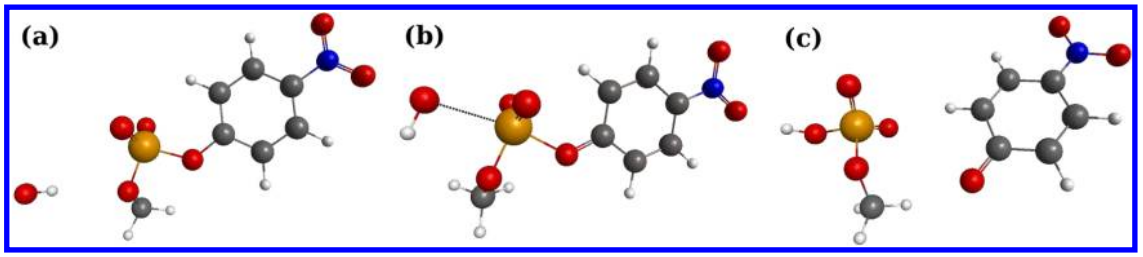

Figure 9. Structures of the solute in the hydrolysis reaction of methyl phenyl phosphate monoanion with a hydroxide ion: (a) reactant, (b) transition state, and (c) product. The *p*-nitro phenyl substituent is shown. All the structures are calculated at the B3LYP/6-31+G(d)/PCM level.

$$HO^- + PO_2(OCH_3)OPhX^- \rightarrow HOPO_2(OCH_3)^- + OPhX^- \quad (52)$$

where X = H (parent compound) or NO_2 (*p*-nitro substituent). The molecular structure is illustrated in Figure 9. This type of reaction is known to be important in signal and energy transduction in living cells.[84] Warshel and co-workers studied the hydrolysis of a series of phosphate diester monoanions by using the COSMO solvation model[85] and the accelerated QM/MM method.[15] They demonstrated that the hydrolysis of methyl phenyl phosphate in eq 52 proceeds via a concerted mechanism through a single transition state (denoted as A_ND_N), and that the calculated activation free energy agrees very well with the experimental result.[15,85] The above reaction thus provides an interesting opportunity to test the reliability of the present MF-QM/MM approach. This is particularly so because the hydroxide ion is known to be difficult to describe accurately with the PC model.[31,32,37]

To proceed, we first calculated an approximate reaction path at the B3LYP/6-31+G(d)/PCM level by using the reaction coordinate

$$\xi = r(P - O_{lg}) - r(P - O_{nuc}) \quad (53)$$

Here, O_{lg} and O_{nuc} denote the oxygen atoms of the leaving group and the nucleophile, respectively. In the path calculation, the reaction coordinate was fixed at a specific value ξ_k, while the remaining degrees of freedom of the QM molecule were fully optimized. The relevant bond lengths at the TS geometry are listed in Table 2. As in the above sections, we calculated the PMF by integrating the QM/MM free energy gradient in eq 40. The QM level was chosen here as MP2/6-311+G(2d,2p), which involves about 500 basis functions for the QM molecule. It is a significant advantage of the MF-QM/MM method that the PMF can be obtained for this size of molecule at a much lower computational cost than the direct QM/MM calculation. Figure 10 presents the PMF profile thus obtained. Not surprisingly, the PC model again exhibited a divergence problem in the self-consistent iterations. On the other hand, the density-based calculation proceeded successfully and provided the PMF shown in Figure 10. The SC model also converged without problem, yielding the PMF similar to the density-based result. The barrier height obtained with the density-based model is $\Delta A^{\ddagger}$ = 21.5 kcal/mol for the parent compound and 19.1 kcal/mol the *p*-nitro substituent. The lower barrier height for the latter is consistent with the smaller pK_a value of *p*-nitro phenol (7.14) than the unsubstituted phenol (9.95). The PMF thus obtained from the MF-QM/MM calculation is similar to that obtained at the B3LYP/6-31+G(d)/PCM level (see Supporting Information), which provides some support for the present use of the approximate reaction path. By adding the solute thermal correction obtained with separable rotation/vibration approximation, we can estimate the free energy of activation as $\Delta G^{\ddagger}$ = 21.5 + 7.5 = 29.0 kcal for the parent compound and $\Delta G^{\ddagger}$ = 19.1 + 7.4 = 26.5 kcal/mol for the *p*-nitro substituent, both of which are in good agreement with the experiment[84] (28.6 and 25.7 kcal/mol). This level of agreement is more than satisfactory considering the approximate nature of the present calculation (particularly the approximate solute thermal correction which may include errors up to 1−2 kcal/mol). The obtained values of free energy are summarized in Table 3. Finally, we display in Figure 11 the SDF of water molecules around the solute molecule. The corresponding RDFs are shown in Supporting Information. The SDF exhibits an excess distribution around the hydroxide and phosphate groups with negative charges. The SDF is rather similar between the parent compound and *p*-nitro substituent, except that an excess distribution appears on top of the *p*-nitro group by reflecting the electron withdrawing character of the latter group.

Table 2. Bond Lengths (in Å) of the Transition State for the Hydrolysis Reaction of Methyl Phenyl Phosphate Monoanions Obtained at the B3LYP/6-31+G(d)/PCM Level[a]

	r(P−O_{nuc})	r(P−O_{lg})
parent	2.27 (1.68)	1.87 (1.69)
p-nitro	2.31 (1.68)	1.91 (1.72)

[a] O_{nuc} and O_{lg} denote the oxygen atom of the nucleophile and leaving groups, respectively. The results for the parent compound and *p*-nitro substituent are shown. The values of r(P−O_{lg}) in parentheses correspond to the reactant state (ξ = −2.8 Å), while the values of r(P−O_{nuc}) in parentheses correspond to the product state (ξ = 2.6 Å).

V. CONCLUDING REMARKS

In this paper, we have described an accurate and efficient implementation of the mean-field QM/MM method based on the continuous charge density of the QM molecule. Our basic motivation here is to improve the description of solute−solvent interactions at short-range. The key ingredients of the implementation are as follows: (i) the grid-based evaluation and interpolation of the ESP (and its gradient) generated by the QM molecule, which allows an efficient statistical sampling of MM molecules, and (ii) the adaptation of the QM/MM-Ewald method of York and co-workers[34] to the mean-field framework, which essentially eliminates cutoff errors in the long-range ES interactions. These techniques allow for a more accurate and reliable treatment of highly charged systems under periodic boundary condition. The conclusions obtained from the present applications in Section IV are as follows:

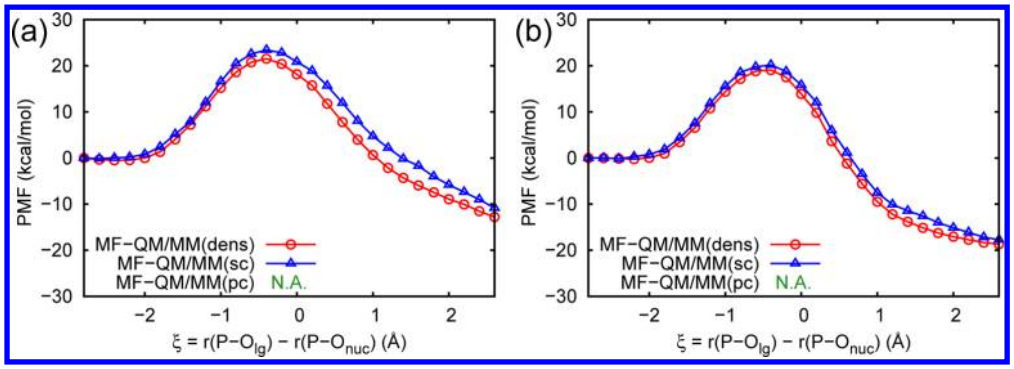

Figure 10. PMF profile of the hydroxide attack on methyl phenyl phosphate monoanions in aqueous solution: (a) the parent compound, (b) *p*-nitro phenyl substituent. The PMF for the MF-QM/MM(pc) calculation is not available because of the divergent behavior of ESP derived charges in the PC model. The QM calculation is performed at the MP2/6-311+G(2d,2p) level.

Table 3. Activation Free Energy $\Delta G^{\ddagger}$ for the Hydrolysis Reaction of Methyl Phenyl Phosphate Monoanions in Aqueous Solution[a]

compd	$\Delta G^{\ddagger}_{expt}$	$\Delta G^{\ddagger}_{calc}$	$\Delta A^{\ddagger}_{MF}$	$\Delta A^{\ddagger}_{slt}$
parent	28.6	29.0	21.5	7.5
4-nitro	25.7	26.5	19.1	7.4

[a] $\Delta A^{\ddagger}_{MF}$ is the barrier height of the PMF profile obtained from the MF-QM/MM(dens) calculation at the MP2/6-311+G(2d,2p) level. $\Delta A^{\ddagger}_{slt}$ denotes the solute thermal correction estimated by the separable rotation/vibration approximation at the B3LYP/6-31+G(d)/PCM level. $\Delta A^{\ddagger}_{calc}$ is calculated as $\Delta A^{\ddagger}_{MF} + \Delta A^{\ddagger}_{slt}$, while $\Delta G^{\ddagger}_{expt}$ denotes the experimental values (ref 84). Energies are given in kcal/mol.

- For the Finkelstein reaction, the point charge approximation gives a PMF rather close to the density-based result. This good agreement is partly due to error cancellation of the point charge approximation along the reaction coordinate. On the other hand, the point charge approximation introduces sizable errors into the (absolute value of) solvation free energy at a given solute geometry.
- For the Menshutkin reaction, the error cancellation is not sufficient to obtain an accurate PMF over the entire reaction coordinate. This is most evident for the product region, in which the solute molecule separates into an ion pair and the degree of solvation is rather different from that of the neutral reactants.
- The situation becomes quite different for reactions in nonaqueous solution (such as acetonitrile). Because of the absence of solute–solvent hydrogen bonds, the penetration effects of the QM molecule is not particularly important compared to aqueous solution. As a result, the obtained PMF agrees very well among the different charge models.
- For phosphate reactions with a large net charge, the point charge approximation exhibits a divergence problem in the self-consistent iterations. In contrast, the density-based calculation proceeds successfully and provides the PMF consistent with experiment. We therefore see that the divergence problem is caused by the neglect of short-range ES damping associated with the QM charge distribution.
- In addition, we have also tested the utility of a recently proposed screened charge model based on the ESP charge operator.[37] Somewhat surprisingly, we have observed that the screened charge calculation not only proceeds in a stable manner but provides the PMF in

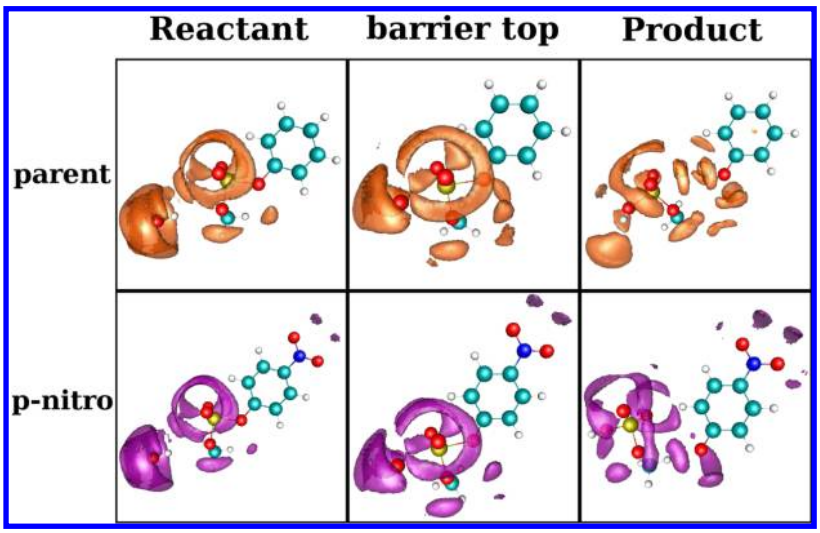

Figure 11. SDFs of water hydrogen around the solute molecule of the hydrolysis reaction of methyl phenyl phosphate monoanions in aqueous solution: (upper panels) the parent compound, (lower panels) *p*-nitro substituent. The isosurfaces are plotted for the number density of 0.30 Å^{-3}, which is equivalent to 4.6 times the average number density of water hydrogen. All the SDFs are obtained from the MF-QM/MM(dens) calculation.

close agreement with the density-based result. This fact again points to the importance of proper short-range damping of the solute−solvent ES interactions.

We would like to further comment on the divergence problem observed in our MF-QM/MM(pc) calculation. The QM charge distribution is approximated by point charges both in the QM and MD calculations. The QM-MM ES interactions are thus overestimated by two factors, namely, by the use of the ESP charge operator in eq 27 and the point-charge approximation for sampling the MM molecules. While we have not explored the degree to which those two factors contribute to the divergence problem, it seems that the ESP charge operator is a more major cause of the problem. This is because several previous studies based on the mean-field approximation do not exhibit such a divergence problem[14,19] (note that in the latter studies the point-charge approximation is used only in the stage of MM sampling). On the other hand, it is also true that MD calculation with point-charge approximation overestimates the QM-MM ES interactions, which is probably the secondary cause of the divergence problem (we recall that point-charge approximation sometimes gives a poor description of the MM distribution for some type of molecules).[22,31] In view of those facts, we expect that a consistent use of QM charge density in both the QM and MD calculations would be beneficial for improving the stability and accuracy of the mean-field QM/MM calculation.

Another concern regarding the solute−solvent interactions is whether one should also consider charge penetration effects of the MM molecules. In fact, this is not a trivial problem because empirical solvent models such as the TIP3P model[42] include penetration as well as polarization effects in an implicit manner. Indeed, we have seen in Section IV that the mean-field QM/MM calculation based on the TIP3P model provides the PMF in good agreement with experiment. We also note that the calculated PMF is not sensitive to the choice of empirical water models.[28] On the other hand, error cancellation may also be operative for the solute−solvent interactions described by the TIP3P model. If this is the case, the use of more accurate water models with finite charge distributions[86−92] may improve the description of absolute solvation properties (such as solvation free energy $\Delta\mu$) to a greater extent than relative properties such as the PMF profile. To see whether this is the case for mean-field QM/MM calculation remains the subject of future study.

APPENDIX A: SCREENED-CHARGE APPROXIMATION TO QM CHARGE DENSITY

The screened-charge (SC) model used in this paper is fully described in ref 37, and thus, only the key expressions are summarized below. (We also note that there are a variety of other screened charge models developed so far in the literature.)[86−92] In the present SC model, we approximate the charge density operator as eq 31, with which the solute charge density is given by

$$\rho(\mathbf{x}) \simeq \langle\Psi|\hat{\rho}^{(\mathrm{sc})}(\mathbf{x})|\Psi\rangle = \sum_a Z_a\delta(\mathbf{x}-\mathbf{R}_a) + \sum_a Q_a^{(e)}F_a(\mathbf{x}) \tag{A1}$$

where $Q_a^{(e)} = \langle\Psi|\hat{Q}_a^{(e)}|\Psi\rangle$ with $\hat{Q}_a^{(e)}$ is the electronic part of the partial charge operator $\hat{Q}_a$. Equation A1 states that the electron distribution is approximately described as the sum of spherical charge distributions $F_a(\mathbf{x})$ centered around each QM atom. We then consider an approximate expression for the total energy given by

$$\tilde{E}_{\mathrm{tot}}(\mathbf{R},\mathbf{r};\tilde{\Psi}) = \langle\tilde{\Psi}|\hat{H}_0 + \int d\mathbf{x}\hat{\rho}^{(\mathrm{sc})}(\mathbf{x})v(\mathbf{x})|\tilde{\Psi}\rangle + E_{\mathrm{QM/MM}}^{\mathrm{vdW}} + E_{\mathrm{MM}} \tag{A2}$$

where $\tilde{\Psi}$, $v(\mathbf{x})$, etc., have the same meaning as defined in Section II.A (here, we assume cluster boundary condition for notational simplicity). Using eq A1, the above $\tilde{E}_{\mathrm{tot}}$ can be rewritten as

$$\tilde{E}_{\mathrm{tot}}(\mathbf{R},\mathbf{r};\tilde{\Psi}) = \langle\tilde{\Psi}|\hat{H}_0 + \sum_a (Z_a v_a + \hat{Q}_a^{(e)} v_a^F)|\tilde{\Psi}\rangle + E_{\mathrm{QM/MM}}^{\mathrm{vdW}} + E_{\mathrm{MM}} \tag{A3}$$

where v_a is the ESP generated by the MM molecules,

$$v_a = v(\mathbf{R}_a) = \sum_i^{\mathrm{MM}} \frac{q_i}{|\mathbf{R}_a - \mathbf{r}_i|} \tag{A4}$$

while v_a^F is its screened counterpart given by

$$v_a^F = \int d\mathbf{x}F_a(\mathbf{x})v(\mathbf{x}) = \sum_i^{\mathrm{MM}} q_i \int d\mathbf{x}\frac{F_a(\mathbf{x})}{|\mathbf{x}-\mathbf{r}_i|} \tag{A5}$$

Based on the total energy in eq A3, we consider an approximate QM/MM free energy given by

$$\tilde{A}^{(\mathrm{sc})}(\mathbf{R},\tilde{\Psi}) = -\frac{1}{\beta}\ln\int d\mathbf{r}^N \exp\{-\beta\tilde{E}_{\mathrm{tot}}(\mathbf{R},\mathbf{r};\tilde{\Psi})\} \tag{A6}$$

and define the mean-field QM/MM free energy $A_{\mathrm{MF}}(\mathbf{R})$ via minimization with respect to $\tilde{\Psi}$, that is,

$$A_{\mathrm{MF}}(\mathbf{R}) = \min_{\tilde{\Psi}} \tilde{A}^{(\mathrm{sc})}(\mathbf{R},\tilde{\Psi}) \tag{A7}$$

The following discussion is essentially the same as in Section II.A. In brief, the effective Schrödinger equation for $\tilde{\Psi}$ is given by eq 32, while the sampling function for the MM part given by eq 33. In this paper, we choose the screening (or smearing) function $F_a(\mathbf{x})$ as a single Slater-type function, $\exp(-\xi_a r)$. The exponent of the latter function, ξ_a, was determined from an ESP fitting procedure similar to the usual charge fitting protocol.[93] For more details of the calculation as well as the analytical expression for v_a^F in eq A5, the reader is referred to ref 37.

APPENDIX B: FREE ENERGY GRADIENT IN THE MEAN-FIELD APPROXIMATION

The free energy gradient $\nabla A_{\mathrm{MF}}(\mathbf{R})$ can be obtained as follows. First, we consider the effective Schrödinger equation for the density-based model,

$$[\hat{H}_0 + \int d\mathbf{x}\hat{\rho}(\mathbf{x})\bar{v}(\mathbf{x})]|\tilde{\Psi}\rangle = \mathcal{E}_{\mathrm{QM}}|\tilde{\Psi}\rangle \tag{B1}$$

where $\bar{v}(\mathbf{x})$ is a short-hand notation for the average MM potential, that is, $\bar{v}(\mathbf{x}) \equiv \langle v(\mathbf{x})\rangle$. The above equation suggests

$$\mathcal{E}_{\mathrm{QM}}(\mathbf{R},\bar{v}) = \langle\tilde{\Psi}|\hat{H}_0|\tilde{\Psi}\rangle + \int d\mathbf{x}\tilde{\rho}(\mathbf{x})\bar{v}(\mathbf{x}) \tag{B2}$$

where $\tilde{\rho}(\mathbf{x})$ is the solute charge density given by $\tilde{\rho}(\mathbf{x}) = \langle\tilde{\Psi}|\hat{\rho}(\mathbf{x})|\tilde{\Psi}\rangle$. Note that $\mathcal{E}_{\mathrm{QM}}$ depends parametrically on the solute geometry $\mathbf{R}$ and the average MM potential $\bar{v}(\mathbf{x})$. With eq B2, one can express the derivative of $A_{\mathrm{MF}}(\mathbf{R})$ as follows:

$$\frac{\partial}{\partial R}A_{\mathrm{MF}}(\mathbf{R}) = \frac{\partial}{\partial R}[\mathcal{E}_{\mathrm{QM}}(\mathbf{R}, \bar{v}) - \int d\mathbf{x}\tilde{\rho}(\mathbf{x})\bar{v}(\mathbf{x}) + \Delta\mu(\mathbf{R}, \tilde{\rho})] \tag{B3}$$

where R is an arbitrary element of $\mathbf{R}$. By noting that $\bar{v}(\mathbf{x})$ depends implicitly on $\mathbf{R}$, we obtain the derivative of $\mathcal{E}_{\mathrm{QM}}$ as follows,

$$\frac{\partial}{\partial R}\mathcal{E}_{\mathrm{QM}}(\mathbf{R}, \bar{v}) = \left.\frac{\partial \mathcal{E}_{\mathrm{QM}}(\mathbf{R}, \bar{v})}{\partial R}\right|_{\bar{v}} + \int d\mathbf{x}\tilde{\rho}(\mathbf{x})\frac{\partial \bar{v}(\mathbf{x})}{\partial R} \tag{B4}$$

where we have used the relation

$$\frac{\delta \mathcal{E}_{\mathrm{QM}}(\mathbf{R}, \bar{v})}{\delta \bar{v}(\mathbf{x})} = \langle\tilde{\Psi}|\hat{\rho}(\mathbf{x})|\tilde{\Psi}\rangle = \tilde{\rho}(\mathbf{x}) \tag{B5}$$

which is obtained by using the Hellmann−Feynman theorem. Likewise, we obtain the derivative of $\Delta\mu$ as

$$\frac{\partial}{\partial R}\Delta\mu(\mathbf{R}, \tilde{\rho}) = \left.\frac{\partial \Delta\mu(\mathbf{R}, \tilde{\rho})}{\partial R}\right|_{\tilde{\rho}} + \int d\mathbf{x}\bar{v}(\mathbf{x})\frac{\partial \tilde{\rho}(\mathbf{x})}{\partial R} \tag{B6}$$

where we have used the relation

$$\frac{\delta \Delta\mu(\mathbf{R}, \tilde{\rho})}{\delta \tilde{\rho}(\mathbf{x})} = \langle v(\mathbf{x})\rangle_{\tilde{\rho}} = \bar{v}(\mathbf{x}) \tag{B7}$$

which follows from the definition of $\Delta\mu$ in eq 16. One can also show the relation

$$\left.\frac{\partial \Delta\mu(\mathbf{R}, \tilde{\rho})}{\partial R}\right|_{\tilde{\rho}} = \left\langle \frac{\partial}{\partial R}E^{\mathrm{vdW}}_{\mathrm{QM/MM}}\right\rangle_{\tilde{\rho}} \tag{B8}$$

By combining the above equations, one can obtain the free energy gradient for nonperiodic systems as follows:

$$\frac{\partial}{\partial R}A_{\mathrm{MF}}(\mathbf{R}) = \left.\frac{\partial \mathcal{E}_{\mathrm{QM}}(\mathbf{R}, \bar{v})}{\partial R}\right|_{\bar{v}} + \left\langle \frac{\partial}{\partial R}E^{\mathrm{vdW}}_{\mathrm{QM/MM}}\right\rangle_{\tilde{\rho}} \tag{B9}$$

By repeating the same arguments with the total energy in eq 17, one can obtain the free energy gradient for periodic systems as given by eq 40.

APPENDIX C: EWALD EXPRESSION FOR THE PERIODIC BOUNDARY CORRECTION TERM

In this paper we evaluated the ΔE^{PBC} term in eq 19 using the Ewald method as follows. First, we write the E_{MM} tem in eq 17 explicitly as

$$E_{\mathrm{MM}} = \frac{1}{2}{\sum_{\mathbf{n}}}' \sum_{i,j}^{\mathrm{MM}} \frac{q_i q_j}{|\mathbf{r}_i - \mathbf{r}_j + \mathbf{n}L|} + E^{\mathrm{excl}}_{\mathrm{MM}} + E^{\mathrm{vdW}}_{\mathrm{MM}} \tag{C1}$$

where $E^{\mathrm{vdW}}_{\mathrm{MM}}$ is the van der Waals potential for MM molecules, and $E^{\mathrm{excl}}_{\mathrm{MM}}$ is the intramolecular exclusion term (we suppose that the MM subsystem consists of rigid molecules such as the TIP3P model). The prime symbol in eq C1 indicates that the $i = j$ term is excluded when $\mathbf{n} = 0$. By combining the above E_{MM} with ΔE^{PBC} in eq 19 and rearranging terms, we have

$$\Delta E^{\mathrm{PBC}} + E_{\mathrm{MM}} = E_{\mathrm{ew}} - \frac{1}{2}\sum_{a\neq b}^{\mathrm{QM}} \frac{\tilde{Q}_a\tilde{Q}_b}{|\mathbf{R}_a - \mathbf{R}_b|} - \sum_{a}^{\mathrm{QM}}\sum_{i}^{\mathrm{MM(I)}} \frac{\tilde{Q}_a q_i}{|\mathbf{R}_a - \mathbf{r}_i|} \tag{C2}$$

where $\{\tilde{Q}_a\}$ and $\{q_i\}$ are QM and MM point charges, respectively, and E_{ew} is given by

$$E_{\mathrm{ew}} = \frac{1}{2}{\sum_{\mathbf{n}}}' \sum_{a,b}^{\mathrm{QM}} \frac{\tilde{Q}_a\tilde{Q}_b}{|\mathbf{R}_a - \mathbf{R}_b + \mathbf{n}L|} + \sum_{\mathbf{n}}\sum_{a}^{\mathrm{QM}}\sum_{i}^{\mathrm{MM}} \frac{\tilde{Q}_a q_i}{|\mathbf{R}_a - \mathbf{r}_i + \mathbf{n}L|} \tag{C3}$$

$$+\frac{1}{2}{\sum_{\mathbf{n}}}' \sum_{i,j}^{\mathrm{MM}} \frac{q_i q_j}{|\mathbf{r}_i - \mathbf{r}_j + \mathbf{n}L|} \tag{C4}$$

The above E_{ew} represents the Coulomb energy for a periodic system consisting of all the coordinates $(\{\mathbf{R}_a\},\{\mathbf{r}_i\})$ and point charges $(\{\tilde{Q}_a\},\{q_i\})$. Thus, it can be evaluated straightforwardly using the standard Ewald method as follows

$$E_{\mathrm{ew}} = E^{(\mathrm{sr})}_{\mathrm{ew}} + E^{(\mathrm{lr})}_{\mathrm{ew}} - \frac{\alpha}{\sqrt{\pi}}\left(\sum_a \tilde{Q}_a^{\,2} + \sum_i q_i^2\right) \tag{C5}$$

where $E^{(\mathrm{sr})}_{\mathrm{ew}}$ is the short-range part of the Ewald energy [as obtained by replacing $1/r$ with $\mathrm{erfc}(\alpha r)/r$], and the long-range part is given by

$$E^{(\mathrm{lr})}_{\mathrm{ew}} = \frac{1}{2V}\sum_{G\neq 0}\frac{4\pi}{G^2}\, e^{-\mathbf{G}^2/4\alpha^2}\left|\sum_a^{\mathrm{QM}} \tilde{Q}_a\, e^{i\mathbf{G}\cdot\mathbf{R}_a} + \sum_i^{\mathrm{MM}} q_i\, e^{i\mathbf{G}\cdot\mathbf{r}_i}\right|^2 \tag{C6}$$

with $V = L^3$ and $\mathbf{G}$ the reciprocal lattice vector. With the above approach, one can evaluate $\Delta E^{\mathrm{PBC}} + E_{\mathrm{MM}}$ efficiently without performing an infinite summation in real space. Using the similar idea, one can obtain the Ewald expression for v^{out}_a in eq 24 as follows:

$$v^{\mathrm{out}}_a = \sum_{\mathbf{n}}\sum_i^{\mathrm{MM}} \frac{q_i\,\mathrm{erfc}(\alpha|\mathbf{R}_a - \mathbf{r}_i + \mathbf{n}L|)}{|\mathbf{R}_a - \mathbf{r}_i + \mathbf{n}L|} + \frac{4\pi}{V}\sum_{\mathbf{G}\neq 0}\frac{e^{-\mathbf{G}^2/4\alpha^2}}{\mathbf{G}^2}\left[\sum_b^{\mathrm{QM}} \tilde{Q}_b\cos\{\mathbf{G}(\mathbf{R}_a - \mathbf{R}_b)\} + \sum_i^{\mathrm{MM}} q_i\cos\{\mathbf{G}(\mathbf{R}_a - \mathbf{r}_i)\}\right] - \sum_{b(\neq a)}^{\mathrm{QM}} \frac{\tilde{Q}_b\,\mathrm{erf}(\alpha|\mathbf{R}_a - \mathbf{R}_b|)}{|\mathbf{R}_a - \mathbf{R}_b|} - \frac{2\alpha}{\sqrt{\pi}}\tilde{Q}_a - \sum_i^{\mathrm{MM(I)}} \frac{q_i}{|\mathbf{R}_a - \mathbf{r}_i|} \tag{C7}$$

ASSOCIATED CONTENT

Supporting Information

Additional PMF profiles as well as the radial distribution functions for the reactions studied in Section IV are provided. This material is available free of charge via the Internet at http://pubs.acs.org/.

AUTHOR INFORMATION

Corresponding Author

*E-mail: yamamoto@kuchem.kyoto-u.ac.jp.

Notes

The authors declare no competing financial interest.

ACKNOWLEDGMENTS

This work was supported by the Grant-in-Aid for Scientific Research (21350010) and that on Innovative Areas (21118508) from the Ministry of Education, Culture, Sports, Science, and Technology (MEXT) of Japan.

REFERENCES

(1) Warshel, A.; Levitt, M. *J. Mol. Biol.* **1976**, *103*, 227.
(2) Field, M. J.; Bash, P. A.; Karplus, M. *J. Comput. Chem.* **1989**, *11*, 700.
(3) Warshel, A. *Computer Modeling of Chemical Reactions in Enzymes and Solutions*; Wiley: New York, 1991.
(4) Muller, R. P.; Warshel, A. *J. Phys. Chem.* **1995**, *99*, 17516.
(5) Plotnikov, N. V.; Kamerlin, S. C. L.; Warshel, A. *J. Phys. Chem. B* **2011**, *115*, 7950.
(6) Higashi, M.; Truhlar, D. G. *J. Chem. Theory Comput.* **2008**, *4*, 790.
(7) Strajbl, M.; Hong, G.; Warshel, A. *J. Phys. Chem.* **2002**, *B 106*, 13333.
(8) Wood, R. H.; Yezdimer, E. M.; Sakane, S.; Barriocanal, J. A.; Doren, D. J. *J. Chem. Phys.* **1999**, *110*, 1329.
(9) Iftimie, R.; Salahub, D.; Wei, D.; Schofield, J. *J. Chem. Phys.* **2000**, *113*, 4852.
(10) Rod, T. H.; Ryde, U. *J. Chem. Theory Comput.* **2005**, *1*, 1240.
(11) Valiev, M.; Garret, B. C.; Tsai, M.-K.; Kowalski, K.; Kathmann, S. M.; Schenter, G. K.; Dupuis, M. *J. Chem. Phys.* **2007**, *127*, 051102.
(12) Chuang, Y.-Y.; Corchado, J. C.; Truhlar, D. G. *J. Phys. Chem. A* **1999**, *103*, 1140.
(13) Ruiz-Pernia, J. J.; Silla, E.; Tunon, I.; Marti, S.; Moliner, V. *J. Phys. Chem. B* **2004**, *108*, 8427.
(14) Rosta, E.; Haranczyk, M.; Chu, Z. T.; Warshel, A. *J. Phys. Chem. B* **2008**, *112*, 5680.
(15) Kamerlin, S. C. L.; Haranczyk, M.; Warshel, A. *Chem. Phys. Chem.* **2009**, *10*, 1125.
(16) Hu, H.; Lu, Z.; Yang, W. *J. Chem. Theory Comput.* **2007**, *3*, 390.
(17) Hu, H.; Lu, Z.; Parks, J. M.; Burger, S. K.; Yang, W. *J. Chem. Phys.* **2008**, *128*, 034105.
(18) Hu, H.; Yang, W. *Annu. Rev. Phys. Chem.* **2008**, *59*, 573.
(19) Fdez. Galvan, I.; Sanchez, M. L.; Martin, M. E.; Olivares del Valle, F. J.; Aguilar, M. A. *J. Chem. Phys.* **2003**, *118*, 255.
(20) Fdez. Galvan, I.; Sanchez, M. L.; Martin, M. E.; Olivares del Valle, F. J.; Aguilar, M. A. *Comput. Phys. Commun.* **2003**, *155*, 244.
(21) Fdez. Galvan, I.; Martin, M. E.; Aguilar, M. A. *J. Comput. Chem.* **2004**, *25*, 1227.
(22) Fdez. Galvan, I.; Martin, M. E.; Aguilar, M. A.; Ruiz-Lopez, M. F. *J. Chem. Phys.* **2006**, *124*, 214504.
(23) Garcia-Prieto, F. F.; Fdez. Galvan, I.; Aguilar, M. A.; Elena Martin, M. *J. Chem. Phys.* **2011**, *135*, 194502.
(24) Tomasi, J.; Mennucci, B.; Cammi, R. *Chem. Rev.* **2005**, *105*, 2999.
(25) Mennucci, B. *WIREs Comput. Mol. Sci.* **2012**, *2*, 386.
(26) Hirata, F., Ed. *Molecular Theory of Solvation*; Kluwer, New York, 2004.
(27) Yamamoto, T. *J. Chem. Phys.* **2008**, *129*, 244104.
(28) Nakano, H.; Yamamoto, T. *J. Chem. Phys.* **2012**, *136*, 134107.
(29) Kosugi, T.; Hayashi, S. *J. Chem. Theory Comput.* **2011**, *8*, 322.
(30) Kosugi, T.; Hayashi, S. *J. Am. Chem. Soc.* **2012**, *134*, 7045.
(31) Takahashi, H.; Takei, S.; Hori, T.; Nitta, T. *J. Mol. Struct.: THEOCHEM* **2003**, *632*, 185.
(32) Takahashi, H.; Ohno, H.; Yamauchi, T.; Kishi, R.; Furukawa, S.; Nakano, M.; Matubayasi, N. *J. Chem. Phys.* **2008**, *128*, 064507.
(33) We have performed similar mean-field QM/MM calculations for methyl diphosphate trianion (MDP^{3-}) and methyl triphosphate tetraanion (MTP^{4-}) in aqueous solution (not reported herein) and found that the latter calculation proceeds successfully without a divergence problem. Thus, it appears that the instability problem depends not only on the total charge of the system but also on various chemical properties such as pK_a of the leaving group as well as the charge distribution of the system.
(34) Nam, K.; Gao, J.; York, D. M. *J. Chem. Theory Comput.* **2005**, *1*, 2.
(35) Ten-no, S.; Hirata, F.; Kato, S. *J. Chem. Phys.* **1994**, *100*, 7443.
(36) Sato, H.; Hirata, F.; Kato, S. *J. Chem. Phys.* **1996**, *105*, 1546.
(37) Nakano, H.; Yamamoto, T. *Chem. Phys. Lett.* **2012**, *546*, 80.
(38) In the case of the SC model, one needs to modify the real-space part of the Ewald method so that it correctly accounts for the short-range attenuation of v_a^F.
(39) Allen, M. P.; Tildesley, D. J. *Computer Simulation of Liquids*; Oxford University, Oxford, 1987.
(40) Coutinho, K.; Georg, H.; Fonseca, T.; Ludwig, V.; Canuto, S. *Chem. Phys. Lett.* **2007**, *437*, 148.
(41) Schmidt, M. W.; Baldridge, K. K.; Boatz, J. A.; Elbert, S. T.; Gordon, M. S.; Jensen, J. H.; Koseki, S.; Matsunaga, N.; Nguyen, K. A.; Su, S.; Windus, T. L.; Dupuis, M.; Montgomery, J. A. *J. Comput. Chem.* **1993**, *14*, 1347.
(42) Jorgensen, W. L.; Chandrasekhar, J.; Madura, J. D.; Impey, R. W.; Klein, M. L. *J. Chem. Phys.* **1983**, *79*, 926.
(43) Cornell, W. D.; Cieplak, P.; Bayly, C. I.; Gould, I. R.; Merz, K. M., Jr.; Ferguson, D. M.; Spellmeyer, D. G.; Fox, T.; Caldwell, J. W.; Kollman, P. A. *J. Am. Chem. Soc.* **1995**, *117*, 5179.
(44) Jorgensen, W. L.; Maxwell, D. S.; Tirado-Rives, J. *J. Am. Chem. Soc.* **1996**, *118*, 11225.
(45) Gao, J.; Xia, X. *J. Am. Chem. Soc.* **1993**, *115*, 9667.
(46) Reichardt, C. *Solvents and Solvent Effects in Organic Chemistry*; Wiley-VCH: Germany, 2003.
(47) Olmstead, W. N.; Brauman, J. I. *J. Phys. Chem. A* **1977**, *99*, 4219.
(48) Chandrasekhar, J.; Smith, S. F.; Jorgensen, W. L. *J. Am. Chem. Soc.* **1985**, *107*, 154.
(49) Chandrasekhar, J.; Jorgensen, W. L. *J. Am. Chem. Soc.* **1985**, *107*, 2974.
(50) Deng, L.; Branchadell, V.; Ziegler, T. *J. Am. Chem. Soc.* **1994**, *116*, 10645.
(51) Truong, T. N.; Stefanovich, E. V. *J. Phys. Chem.* **1995**, *99*, 14700.
(52) Pomelli, C. S.; Tomasi, J. *J. Phys. Chem. A* **1997**, *101*, 3561.
(53) Sato, H.; Sakaki, S. *J. Phys. Chem. A* **2004**, *108*, 1629.
(54) Vayner, G.; Houk, K. N.; Jorgensen, W. L.; Brauman, J. I. *J. Am. Chem. Soc.* **2004**, *126*, 9054.
(55) Freedman, H.; Truong, T. N. *J. Phys. Chem. B* **2005**, *109*, 4726.
(56) Ardura, D.; Ĺopez, R.; Sordo, T. L. *J. Phys. Chem. B* **2005**, *109*, 23618.
(57) Higashi, M.; Truhlar, D. G. *J. Chem. Theory Comput.* **2008**, *4*, 1032.
(58) Su, P.; Wu, W.; Kelly, C. P.; Cramer, C. J.; Truhlar, D. G. *J. Phys. Chem. A* **2008**, *112*, 12761.
(59) Lu, Z.; Zhang, Y. *J. Chem. Theory Comput.* **2008**, *4*, 1237.
(60) *Theoretical Aspects of Physical Organic Chemistry*; Shaik, S. S., Schlegel, H. B., Wolfe, S., Eds.; Wiley: New York, 1992.
(61) In actual calculations, we utilized appropriate expressions for $\Delta\mu_{es}$ for periodic systems.
(62) Böhm, H. J.; McDonald, I. R.; Madden, P. A. *Mol. Phys.* **1983**, *49*, 347.
(63) Amovilli, C.; Mennucci, B.; Floris, F. M. *J. Phys. Chem. B* **1998**, *102*, 3023.
(64) Gao, J. *J. Am. Chem. Soc.* **1991**, *113*, 7796.
(65) Shaik, S.; Ioffe, A.; Reddy, A. C.; Pross, A. *J. Am. Chem. Soc.* **1994**, *116*, 262.
(66) Dillet, V.; Rinaldi, D.; Bertran, J.; Rivail, J.-L. *J. Chem. Phys.* **1996**, *104*, 9437.
(67) Truong, T. N.; Truong, T. T.; Stefanovich, E. V. *J. Chem. Phys.* **1997**, *107*, 1881.

(68) Webb, S. P.; Gordon, M. S. *J. Phys. Chem. A* **1999**, *103*, 1265.
(69) Hirao, H.; Nagae, Y.; Nagaoka, M. *Chem. Phys. Lett.* **2001**, *348*, 350.
(70) Marti, S.; Moliner, V. *J. Chem. Theory Comput.* **2005**, *1*, 1008.
(71) Komeiji, Y.; Ishikawa, T.; Mochizuki, Y.; Yamataka, H.; Nakano, T. *J. Comput. Chem.* **2009**, *30*, 40.
(72) Acevedo, O.; Jorgensen, W. L. *J. Phys. Chem. B* **2010**, *114*, 8425.
(73) The force constant K_m (in kcal/mol·Å^2) for the umbrella potential centered at the reaction coordinate ξ_m (in Å) was given as follows: (ξ_m, K_m) = (−1.2, 80), (−1.0, 100), (−0.8, 120), (−0.6, 140), (−0.4, 160), (−0.2, 180), (1.4, 180), (1.6, 160), (1.8, 140), (2.0, 120), while K_m = 50 for $-2.2 \le \xi_m \le -1.2$ and K_m = 200 for $0.0 \le \xi_m \le 1.2$.
(74) Cramer, C. J. *Essentials of Computational Chemistry*; Wiley: New York, 2002.
(75) Kim, Y.; Mohrig, J. R.; Truhlar, D. G. *J. Am. Chem. Soc.* **2010**, *132*, 11071.
(76) Ribeiro, R. F.; Marenich, A. V.; Cramer, C. J.; Truhlar, D. G. *J. Phys. Chem. B* **2011**, *115*, 14556.
(77) Admiraal, S. J.; Herschlag, D. *Chem. Biol.* **1995**, *2*, 729.
(78) Wolfenden, R. *Chem. Rev.* **2006**, *106*, 3379.
(79) Guthrie, J. P. *J. Am. Chem. Soc.* **1977**, *99*, 3991.
(80) The reason for using the BHHLYP/6-31+G(d,p)/COSMO method for solute thermal correction is that the MP2/6-31+G(d,p)/COSMO method failed to determine the precise location of the transition state. The latter failure may be due to the flatness of the free energy surface in the transition-state region.
(81) Lad, C.; Williams, N. H.; Wolfenden, R. *Proc. Natl. Acad. Sci. U.S.A.* **2003**, *100*, 5607.
(82) K̈lahn, M.; Rosta, E.; Warshel, A. *J. Am. Chem. Soc.* **2006**, *128*, 15310.
(83) Li, W.; Rudack, T.; Gerwert, K.; G̈rater, F.; Schlitter, J. *J. Chem. Theory Comput.* **2012**, *8*, 3596.
(84) Zalatan, J. G.; Herschlag, D. *J. Am. Chem. Soc.* **2006**, *128*, 1293.
(85) Rosta, E.; Kamerlin, C. L.; Warshel, A. *Biochemistry* **2008**, *47*, 3725.
(86) Freitag, M. A.; Gordon, M. S.; Jensen, J. H.; Stevens, W. J. *J. Chem. Phys.* **2000**, *112*, 7300.
(87) Slipchenko, L. V.; Gordon, M. S. *Mol. Phys.* **2009**, *107*, 999.
(88) Cisneros, G. A.; Tholander, S. N.; Parisel, O.; Darden, T. A.; Elking, D.; Perera, L.; Pique-mal, J. P. *Int. J. Quantum Chem.* **2008**, *108*, 1905.
(89) Werneck, A. S.; Filho, T. M. R.; Dardenne, L. E. *J. Phys. Chem. A* **2008**, *112*, 268.
(90) Wang, B.; Truhlar, D. G. *J. Chem. Theory Comput.* **2010**, *6*, 3330.
(91) Andres Cisneros, G.; Piquemal, J.-P.; Darden, T. A. *J. Chem. Phys.* **2006**, *125*, 184101.
(92) Elking, D. M.; Andres Cisneros, G.; Piquemal, J.-P.; Darden, T. A.; Pederson, L. G. *J. Chem. Theory Comput.* **2010**, *6*, 190.
(93) Bayly, C. I.; Cieplak, P.; Cornell, W.; Kollman, P. A. *J. Phys. Chem.* **1993**, *97*, 10269.